Efficient Thermally Activated Delayed Fluorescence Molecules Utilizing Donor-Acceptor Structure and Their Application for Highly Efficient Organic Light Emitting Diodes

李, 博

Efficient Thermally Activated Delayed Fluorescence Molecules Utilizing Donor-Acceptor Structure and Their Application for Highly Efficient Organic Light Emitting Diodes

Department of Chemistry and Biochemistry

Graduate School of Engineering

Kyushu University

Bo Li

Chapter 1

Introduction

1.1 A brief history of organic light emitting diodes (OLEDs)

The possibility of practical utilization of organic electroluminescence (EL) was not taken into consideration until J. Dresner reported a double injection EL device based on anthracene single crystals.[1] However, other early attempts mainly based on single crystal showed that it required a quite high driven voltage of over 100 V, suggesting that organic EL was far from practical application.[2-15]

By taking disadvantage of the single crystal based OLEDs, thin−film OLEDs fabricated by vacuum deposition were extensively studied aimed for mainly low driving voltage in 1980'.[16-20] In 1983, R. H. Partridge et al. reported the first double−layered thin−film OLEDs consisting of a poly(N-vinyl carbazole) (**PVCz**) emitting layer.[21-24] In 1986, further, S. Hayashi et al. dramatically decreased the threshold voltage of an EL device down to 4 V by using electropolymerized polythiophene as a hole injection layer (HIL) and a vacuum deposited perylene film as an emitting material layer (EML).[25] In particular, the current prototype structure of OLEDs was established in 1987, when C. W. Tang et al. reported a novel thin-film double-layered structure.[26] In this device, a fluorescent metal chelate complex, tris(8-hydroxyquinoline) aluminum (**AlQ$_3$**), was used as a light emitting and electron-transport layer, while a diamine layer was used as a hole-transport layer (HTL). At that time, this diode realized rather high external quantum efficiency (EQE) of 1% and high luminesce of over 1000 cd/m^2 at a driving voltage below 10 V. To facilitate charge injection and transfer into the emissive region, a fundamental three-layer structure consisting of a HTL, an EML and an electron-transport layer (ETL) was well established by C. Adachi et al. in 1988, which becomes the most generally used OLED structure so far.[27] In 1990, in a similar manner, J. H. Burroughes et al. utilized conjugated polymers as an active material in OLEDs, demonstrating OLED fabrication based on wet-processing.[28]

In these first generation OLEDs, only a small fraction (25%) of electrically

generated excitons induced light emission due to the limitation of the spin statistics in fluorescent dyes. On the other hand, to harvest both singlet and triplet excitons, S. R. Forrest and M. E. Thompson et al. employed room-temperature phosphorescent dyes into an active layer.[29] Novel metal atoms in phosphors caused strong spin-orbital coupling, facilitating the radiative decay from triplet into ground states. After comprehensive optimization of materials and device structures, nearly 100% internal quantum efficiency (IQE) was realized in 2000.[30]

These pioneer studies demonstrated high potential of OLEDs as an alternative of display and lighting technology. After that, a considerable amount of effort has been devoted to improve the efficiency and stability of OLEDs.

1.2 Work mechanism and structure of OLEDs

The current standard OLEDs consist of multiple organic and metallic layers on a transparent substrate. Small molecular organic and metallic layers are usually deposited by thermal evaporation, while polymer layers are prepared by solution processes such as spin-coating and inkjet printing techniques. Chemical stability, especially the resistance to oxidation under the process of device fabrication and operation under electrical excitation, is requisite for all organic layers and a wide variety of molecular structures have been examined.

A typical OLED structure contains single- or multiple-organic layers sandwiched between an anode and a cathode, in which at least one electrode should be transparent for light out-coupling (Fig. 1-1). In the case of single layer OLEDs,[2] an organic layer serves as both light emitting source and charge transfer layer, and requires high photoluminescence quantum yield (PLQY) and bipolar charge-transport property. However, most EL materials are unipolar, i.e., only hole transport or electron transport. In order to prevent the emission quenching near the cathode, an opposing unipolar conductive layer is inserted so that the electron-hole recombination

zone can be confined near the interface of two organic layers.[26] More recent developments in OLED structures improved the device efficiency and stability by reducing carrier injection barrier at the interfaces of electrode/organic layers. In some devices, independent hole and electron injection layers (HIL and EIL) are applied to aid charge injection at electrodes and achieve the desired performance. In particular, higher injection current can be made by using a p-i-n structure with p-doping in the HIL and n-doping in the EIL. In 1998, K. Leo's group proposed a structure using vanadyl phthalocyanine (**VOPc**) doped with 2,3,5,6-tetrafluoro-7,7,8,8-tetracyano quinodimethane (**F4-TCNQ**) as a HTL to decrease driving voltage.[31] In 2004, they finally developed a device with p-i-n structure, where N,N,N',N'-tetrakis(4-methoxyphenyl)-benzidine (**MeO-TPD**) doped with **F4-TCNQ** was used as a p-doped hole injection and transport layer, 4,7-diphenyl-1,10-phenanthroline (**Bphen**) and cesium were coevaporated as a n-doped electron transport layer, and an intrinsic EML was sandwiched between these two doped layers.[32] Such a pin OLED achieved a maximum power efficiency of 53 lm/W and a power efficiency of 45 lm/W at a luminance of 1000 cd/m^2.
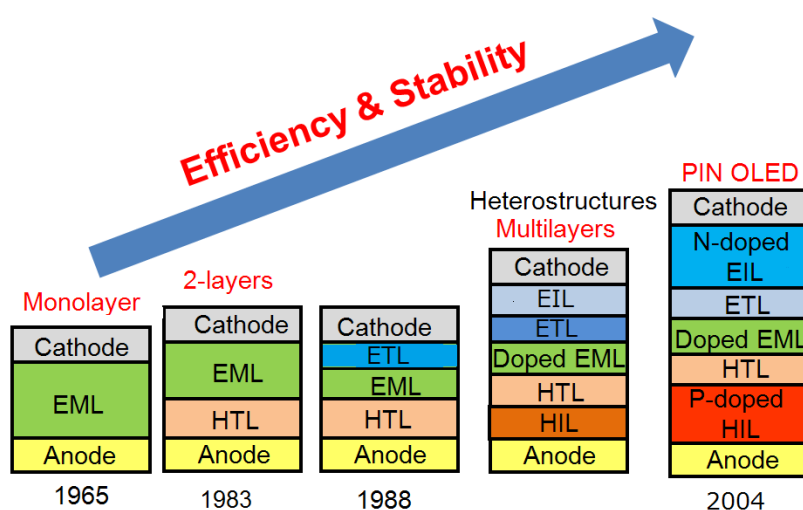

Figure 1-1. Evolution of OLED structures.[33] (EML: emitting material layer; HTL: hole transport layer; ETL: electron transport layer; EIL: electron injection layer; HIL: hole injection layer.)

Simultaneously, carrier injection electrodes were also developed. Currently, the most useful anode is indium-tin-oxide (**ITO**) which has appropriate work function (-5.0 eV) favorable for hole injection and low-work-function metals such as Al:Li, Mg:Ag alloys[34] and an Al/LiF multilayer are widely used as cathode.

1.3 Emitting materials in OLEDs – Small molecule fluorophors and phosphors

The efficiency of an OLED can be characterized by its quantum efficiency (photon/electron). The values of external quantum efficiency (η_{ext}) and internal quantum efficiency (η_{int}) are two important factors to clarify OLED performance. The η_{ext} is defined as the ratio of the number of photons emitted from the device to the number of injected electrons and is given by:

$$\eta_{ext}=\Phi_F\,\chi\gamma\eta_{out}=\eta_{int}\eta_{out}$$

where Φ_F is the intrinsic PL efficiency; χ is exciton branching ratio; γ is the charge balance factor, which can be assumed to be unity in the case of well-balanced carrier injection and transport; η_{out} is the light out-coupling efficiency estimated to be 0.2-0.3. Fluorophors and phosphors are the two dominant categories of small molecular light emitting materials for OLEDs. Fluorescent materials represented by **AlQ$_3$** are the first generation of OLED light emitting materials, which show radiative decay from the lowest singlet excited state (S$_1$) to the ground state (S$_0$), i.e., fluorescence. They are usually low cost and have high reliability. However, poor singlet generation fraction (25%) limits the η_{ext} to be approximately 5% for fluorescent OLEDs.

Phosphorescence is defined as a radiative transition from the lowest triplet excited state (T$_1$) to S$_0$. Since this process is usually forbidden by spin multiplicity selection rules, it can happen only in polymers where the interchain bond-charge correlation has a strong influence on singlet and triplet excitons generation ratio[35, 36] or organometallic compounds containing heavy atoms where the excited states are not

purely a singlet or triplet state due to enhanced spin-orbit coupling [37-40].

   While spin-forbidden phosphorescence has a much smaller rate constant (10^0-10^6 s^{-1}) than that of fluorescence (10^6-10^9 s^{-1}), OLEDs applying room temperature phosphorescent materials such as iridium(2-phenylpyridine)$_3$ (**Ir(ppy)$_3$**) have achieved 100% internal efficiency,[40] which can be attributed to all harvesting of triplet excitons. However, phosphorescence OLEDs have some serious issues to be improved. With an increase of current density, a significant efficiency roll-off can be observed, caused by an increase of nonradiative decay and triplet-triplet annihilation (TTA) during long lifetime of the triplet excitons. Furthermore, the use of rare metals also increases the cost in commercial application.

   Some classical fluorescent and phosphorescent small molecules utilized in OLEDs are showed in Fig. 1-2. Among them, 4-dicyanm-ethylene-2-methyl-6-(p-dimethylaminostyryl)-4H-pyran (**DCM**),[41] (4-(dicyanomethylene)-2-tert-butyl-6-(1,1′,7,7′-tetramethyljulolidin-4-yl-vinyl)-4H-pyran) (**DCJTB**),[42] 5,6,11,12-tetraphenylnaphthacene (**rubrene**),[41] and tetraphenyldibenzoperiflanthene (**DBP**)[43] emit red fluorescence, **AlQ$_3$**,[27] N,N'-Dimethyl quinacridone (**DMQA**),[41] 10-(2-benzothiazolyl)-1,1,7,7-tetramethyl-2,3,6,7-tetrahydro-1H,5H,11H-benzo[l] pyrano[6,7,8-i,j]quinolizin-11-one (**C545T**),[44] coumarin 6 (**Co-6**),[45] and 9,10-bis [phenyl(m-tolyl)-amino]anthracene (**TPA**)[46] emit green fluorescence, while perylene,[47] 4,4′-bis(2,2'-diphenyl-ethene-1-yl)-diphenyl (**BPVBi**),[48,49] and 4-(di-p-tolylamino)-4'-[(di-p-tolylamino)styryl]stilbene (**DPAVB**)[50] emit red fluorescence. Platinum-octaethyl-porphyrin (**PtOEP**) is the first phosphorescent emitter employed in OLEDs.[51] However, iridium (III) complexes are currently the most widely used phosphors. The red, green and blue phosphorescent OLEDs based on tris(1-phenyl isoquinolinolato-C2,N)iridium(III) (**Ir(piq)$_3$**), fac-tris(2-phenylpyridine) iridium (**(ppy)$_2$Ir(acac)**) and bis[(4,6-difluorophenyl) pyridinato-N,C2](picolinato) iridium (**FIrpic**) have achieved EQEs of 10.3%, 19% and 22%, respectively.[30,52,53]

Fluorescent Emitters
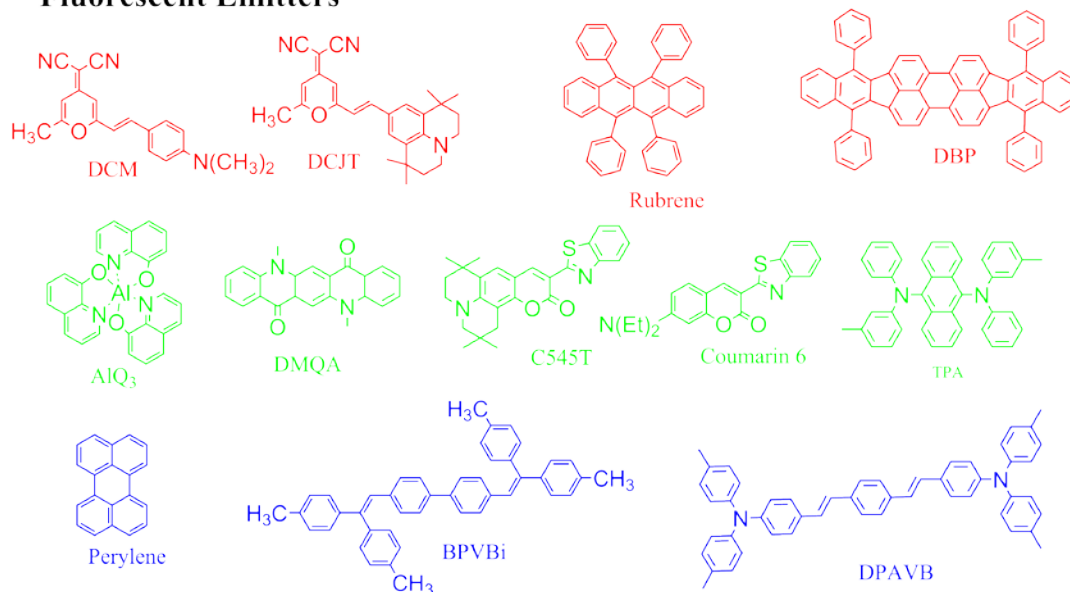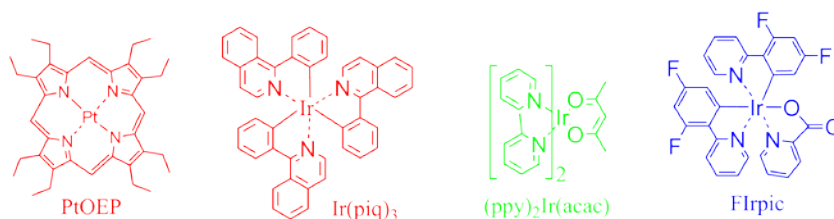

Phosphorescent Emitters

Figure 1-2. Chemical structures of small molecular light emitting materials utilized in OLEDs.

1.4 Light emitting materials in OLEDs –Polymer and Dendrimer

One of the key disadvantages of small molecular OLEDs is the cost for device fabrication, because they require rather expensive vacuum deposition system with high vacuum level. On the other hand, unlike small molecules, polymer films can be fabricated from solution processes such as spin-coating or ink-jet printing methods. In 1990, R. Friend et al. demonstrated the first efficient polymer OLED based on poly(p-phenylene vinylene) (**PPV**, Fig. 1-3).[28] After that, they further extended the **PPV** system by using different 2,5-substituent groups to control the state of order and get poly(2,5-dimethoxy-p-phenylene vinylene) (**PDMeOPV**). The introduction of methoxy substituents allows regular arrangement to form a three-dimensional

structure.[42] In 1992, G. Gustafsson et al. fabricated the first flexible PLEDs by using poly(2-methoxy-5-(2'-ethyl)-hexoxy-1,4-phenylene vinylene) (**MEH-PPV**).[43] Besides **PPV** backbone, thiophene-based conjugated polymers also attracted extensively interests for soluble and processable merits. The first synthesis of coupled poly(3-alkylthiophene) (**P3AT**) was reported by R. D. McCullough in 1992.[44, 45]
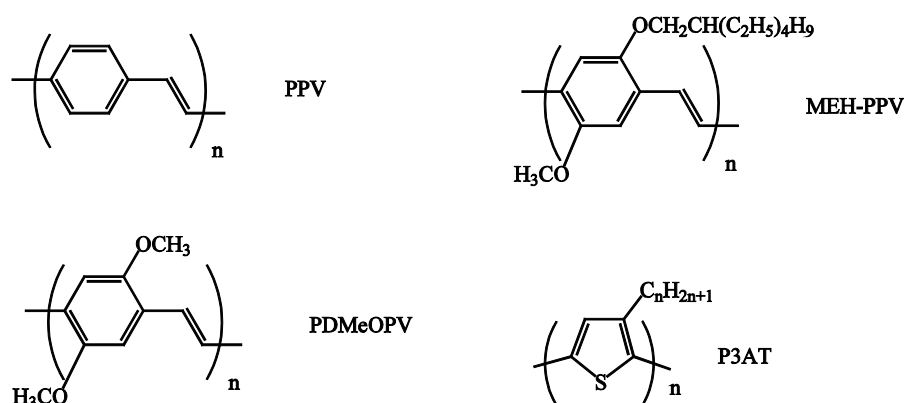

Figure 1-3. Chemical structures of selected conjugated polymer EL materials: **PPV**, **PDMeOPV**, **MEH-PPV**, **P3AT**.

In polymers, I note that the maximum quantum efficiencies of EL and photoluminescence (PL) can theoretically approach unity when the electron-hole binding energy is sufficiently weak.[35] Z. Shuai et al. provided a theoretical model of singlet state formation ratio in polymers, suggesting that singlet exciton formation is proportion to their π-conjugated length[36, 46-48] and this has been well confirmed by some experiments.[49-54]

Besides small molecules and polymers, dendrimers have also attracted considerable attraction for their merits, such as ordered, covalent three-dimensional structures, resulting in spatial controllability of active components.[55-65] EL from a single-component emitting layer of dendritic macromolecules was reported by P. W. Wang et al. in 1996.[66] Light emitting dendrimers can be categorized into two categories: fully conjugated ones[57, 59, 66] and chromophores with dendron

8

non-conjugated substitutions.[62, 67, 68] The light emitting characteristics and processing properties of dendrimers can be controlled by chromophores and surface substitutions independently. In high generation dendrimers, the interaction between neighbor molecules is strongly influenced by surface groups. Consequently, the aggregation induced quenching can be avoided. The optical energy gap near the surface and near the core can also be adjusted respectively to accelerate the mobility of charges and excitons in it.[69, 70]
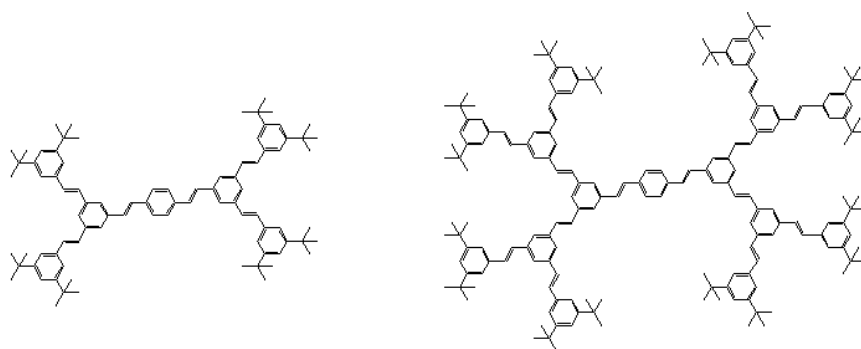

Figure 1-4. Conjugated dendrimers consisting of a distyrylbenzene core (short wavelength emission), stilbene dendrons (charge transport), and tert-butyl surface groups (good process ability).[57]
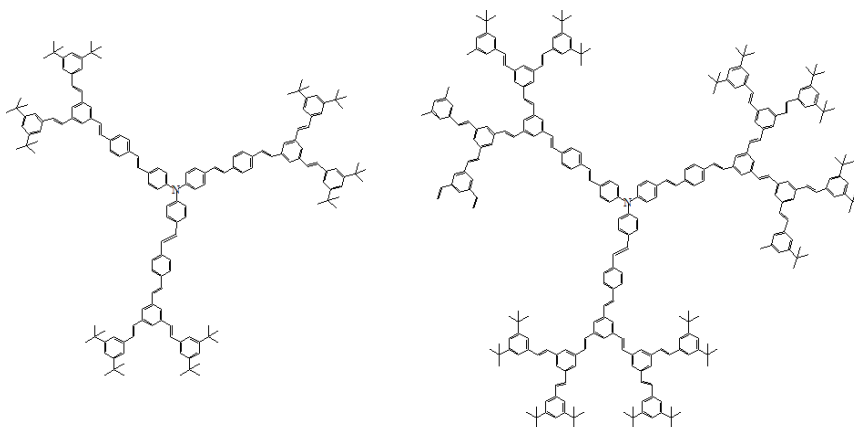

Figure 1-5. Samuel and co-workers synthesized the triphenylamine based dendrimers decorated by three distyrylbenzene chromophores and demonstrated that the degree of the interaction of the molecules is controlled by the generation.[71]

1.5 Novel approaches to improve device efficiency

While fluorescent materials possess merits of low cost and high stability, they suffer from shortcoming of low EL efficiency limited by the spin statistics. Therefore,

significant progresses have been made in developing new materials and device systems that can overcome the spin statistical limit of fluorescent materials.

To make triplet states in fluorescent materials available, two possible approaches are identified. One is triplet–triplet annihilation (TTA),[38, 72-93] and the other one is thermally activated delayed fluorescence (TADF).[78, 94-109] In the TTA process, the confliction between two triplet excitons can produce a singlet exciton. Thus, the upper η_{int} limit of OLEDs using TTA process can increase up to 63% (0.25+0.75×0.5). Assuming that the optical outcoupling efficiency is 0.20, the maximum external quantum efficiency (EQE) is estimated to be 13%. In 2009, the EQE of TTA devices was reported to be 11%, which is very close to the theoretical limitation.[74] On the other hand, triplets can also be converted to singlets by reverse intersystem crossing (RISC) under thermal activation when the energy difference between S_1 and T_1 excited states (ΔE_{ST}) is small enough.[110, 111]

TADF was observed by S. J. Boudi in 1930 and elucidated by C. A. Parker and C. G. Hatchard in 1961.[112] This phenomena was also observed in some kinds of fullerene,[112,113] and metal complexes.[114] In 2009, A. Endo et al. in our group proposed TADF based OLEDs for the first time using some Sn^{4+}-porphyrin complexes. However, the efficiencies of these devices were still low (EQE=0.3%).[115] In a later work, K. Goushi et al. used intermolecular charge transfer (CT) molecules, i.e., exciplex, to realize a small overlap between donor and acceptor wavefunctions.[116] However, the forbidden transition nature also resulted in a rather low fluorescent rate, and consequently, relatively limited PL and EL efficiencies. To break this bottleneck, our group considered intramolecular CT materials with intra molecular donor-acceptor structures. In 2011, A. Endo et al. demonstrated an efficient TADF based OLEDs containing 2-biphenyl-4,6-bis(12-phenylindolo[2,3-a]carbazole-11-yl) -1,3,5-triazine (**PIC-TRZ**), in which a maximum EQE of 5.3% was obtained with a relatively low PLQY of 39%.[109] In the same year, T. Nakagawa et al. proposed a TADF molecule based on spirobifluorene derivatives, i.e., 2′,7′-bis(di-*p*-tolyl

amino)-9,9′ - spirobifluorene-2,7-dicarbonitrile (**Spiro-CN**).[106] In this device, TADF components contributed over half of the EQE. After that, comprehensive surveys of TADF materials with high efficiency were conducted. H. Tanaka et al. reported a green TADF emitter, phenoxazine-triphenyltriazine (**PXZ-TRZ**), with a maximum EQE of 12.5%.[105] In 2012, the green TADF device with an emission peak at 520 nm finally reached an EQE (19.5%) that is comparable to the best phosphorescent OLEDs by using a carbazolyl dicyanobenzene emitter (1,2,3,5-tetrakis(carbazol-9-yl)-4,6-dicyanobenzene, **4CzIPN**).[104] Efficient blue and orange TADF materials were also successfully synthesized, with maximum EQE of 10% and 17.5%, respectively.[100, 103] The molecular structures are shown in Fig. 1-6.
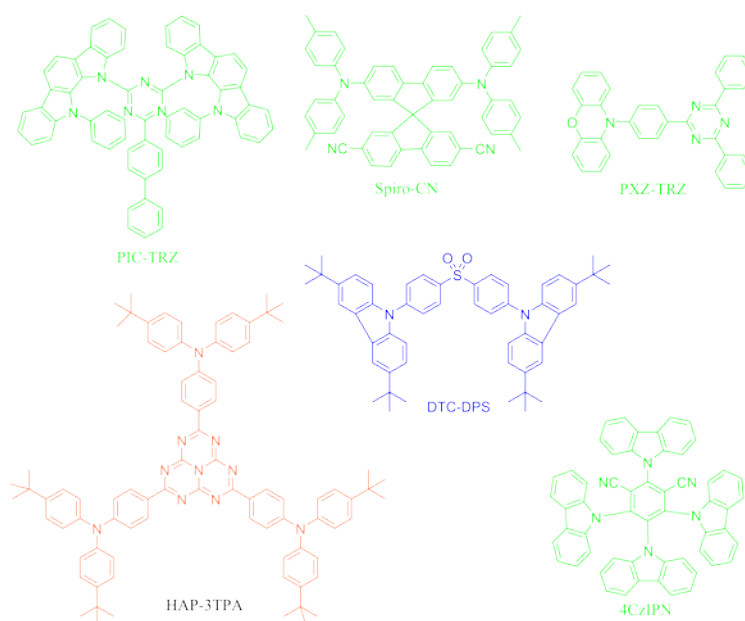

Figure 1-6. Chemical structures of some TADF molecules utilized in OLEDs.

1.6 Mechanism of thermally activated delayed fluorescence (TADF)

After excitation by photons, radiative and nonradiative deactivation processes take place in a molecule. Nonradiative internal conversion (IC) between two states of equal spin multiplicity, S_n and S_1, or T_n and T_1, is very fast among the excited states.

At the same time, the transitions between two states with different multiplicities (intersystem conversion, ISC) also compete with these photophysical relaxation processes. A radiative transition from the lowest singlet excited state to the ground state is fluorescence. To be more precise, it should be called prompt fluorescence (PF). For common closed-shell molecules, the states involved in the fluorescence process are S_0 (ground singlet state) and usually S_1 (first excited singlet). In addition, fluorescence also occurs via the triplet manifold: electrons excited to S_1 and decay to T_1 through an intersystem crossing. After vibrational thermalization, a reverse intersystem crossing back to S_1 occurs, resulted in delayed fluorescence (DF). Here, interconversion between the singlet and triplet excited states would repeat multiple times before the excitons get final decay from singlet or triplet excited states.[113] A simple scheme of this process is shown in Fig. 1-7.
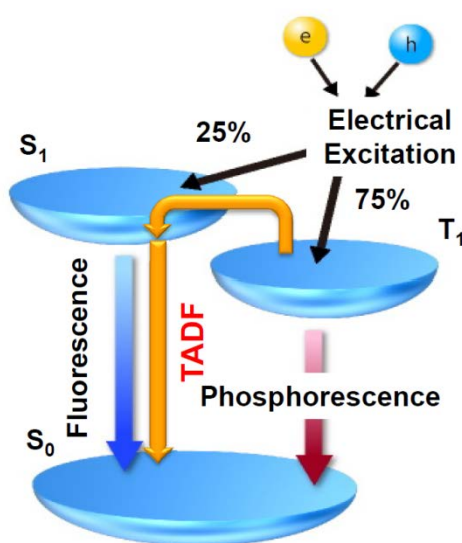

Figure 1-7. Scheme of TADF process.

Referring to the prompt fluorescence, this second type of fluorescence is named thermally activated delayed fluorescence (TADF). Two conditions should be met for significant TADF to occur: (i) reasonably high probability of S_1 to T_1 intersystem crossing ($k_{ISC} >> k_F + k^S_G$), and (ii) reasonably high probability of subsequent T_1 to S_1

reverse intersystem crossing ($k_{RISC} \gg k_P + k^T_G$).[117] In most cases, it is also observed that $k_{ISC} \gg k_{RISC}$ and $k^T_G \gg k_P$. The model for these processes can be simply illustrated by a three-state system.
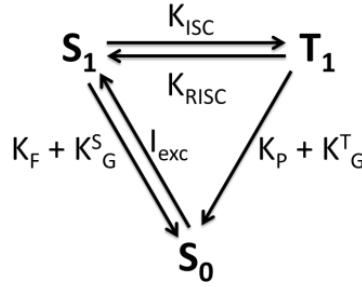

Figure 1-8. Kinetic scheme for TADF

Here, I_{exc} stands for excitation intensity, k_F and k_P denote radiative rate constants of fluorescence and phosphorescence, respectively, k^S_G and k^T_G are the nonradiative rate constants for deactivation to the ground state, k_{ISC} and k_{RISC} are the intersystem crossing (ISC) and reverse intersystem crossing (RISC) rate constant, respectively. The RISC rate constant (k_{RISC}) is given by equation (1).[118]

$$k_{RISC} = \frac{\sum_v k_v exp(-\frac{E_v}{k_B T})}{\sum_v exp(-\frac{E_v}{k_B T})} \quad (1)$$

where k_v is the RISC rate constant of the vth vibrational level of T_1 (v is an integer which represents the vibrational quantum numbers) and E_v is the respective vibrational energy. Assuming that k_v is a step function and ΔE_{ST} is the S_1-T_1 energy splitting, and the energy difference between consecutive vibronic levels is much smaller than $k_B T$, and the density of states is approximately constant, equation (1) becomes,

$$k_{RISC}(T) = exp(-\frac{\Delta E_v}{k_B T}) \quad (2)$$

Different assumptions on k_v and on the density of vibrational states lead to a weak

temperature dependence of the pre-exponential factor. Owing to the relative energies of S_1 and T_1, the triplet-to-singlet RISC rate constant is always an activated process that is strongly temperature dependent.[114, 119-122]

1.7. Aim of this research

Inexpensive TADF aromatic compounds have emerged as attractive alternatives to phosphorescent complexes for OLED applications. The most critical design strategy of TADF molecules is to reach a small ΔE_{ST}. According to the previous study of our group, well separation of the highest occupied and lowest unoccupied molecular orbitals (HOMO and LUMO) is favorable to realizing TADF in organic aromatic compounds.[105, 106, 109] Emitters characterized by pretwisted intramolecular charge transfer (ICT) meet with this requirement because the large twist angle between donor and acceptor moieties limits their electronic interaction and minimizes the overlap of the orbitals involved in the transitions. On the basis of this design strategy, a series of green TADF emitters that can exhibit near-unity internal quantum efficiency (IQE) in devices were recently developed by our group.[104]

One objective of this thesis is to develop novel pretwisted ICT type TADF emitters for full-color display, especially the high performance blue TADF emitters. We know that the emission color of donor-acceptor (D-A) structured molecules can be tunable by adjusting redox potential of the donor and acceptor moieties. In this thesis, novel pretwisted ICT molecules with various acceptor and donor moieties were synthesized and characterized. Another objective of this thesis is to solve the efficiency roll-off problem found in most blue TADF OLEDs, which is primarily caused by the relatively large ΔE_{ST} and the long excited-state lifetime of the emitters.[103, 104] In this thesis, a three-excited-state model involving an emissive ^1CT state, spin forbidden ^3CT and locally excited triplet (^3LE) states was proposed to describe the low lying excited states of the investigated molecules. I demonstrate that

the energy relationships of these three excited states can be well controlled through a deep understanding of the structure–property relationships in TADF emitters, and efficient and short-lifetime blue TADF emitters can be finally achieved in this study.

References

1. Dresner, J., Double Injection Electroluminescence in Anthracene. *Rca Rev* **1969,** *30*, 322-334.

2. Pope, M.; Magnante, P.; Kallmann, H. P., Electroluminescence in Organic Crystals. *J. Chem. Phys.* **1963,** *38*, 2042-2043.

3. Helfrich, W.; Schneide, W. G., Recombination Radiation in Anthracene Crystals. *Phys. Rev. Lett.* **1965,** *14*, 229.

4. Williams, D. F.; Schadt, M., Dc and Pulsed Electroluminescence in Anthracene and Doped Anthracene Crystals. *J. Chem. Phys.* **1970,** *53*, 3480.

5. Helfrich, W.; Schneider, W. G., Transients of Volume‐Controlled Current and of Recombination Radiation in Anthracene. *The Journal of Chemical Physics* **1966,** *44*, 2902-2909.

6. Sano, M.; Pope, M.; Kallmann, H., Electroluminescence and Band Gap in Anthracene. *The Journal of Chemical Physics* **1965,** *43*, 2920-2921.

7. Werner, T. C.; Chang, J.; Hercules, D. M., Electrochemiluminescence of anthracene and 9,10-dimethylanthracene. Role of direct excimer formation. *J. Am. Chem. Soc.* **1970,** *92*, 763-768.

8. Schwob, H. P.; Weitz, D.; Williams, D. F., The Variation of the Carrier Recombination Region with Carrier Density in Anthracene Crystals. *Mol Cryst Liq Cryst* **1973,** *24*, 271-282.

9. Kalinowski, J.; Godlewski, J.; Signerski, R., Electroluminescence in Tetracene Crystals. *Mol Cryst Liq Cryst* **1976,** *33*, 247-259.

10. Gliński, J.; Godlewski, J.; Kalinowski, J., Spatial Distribution of the Distribution of the Electroluminescence and the Recombination Process in Tetracene Single Crystals. *Mol Cryst Liq Cryst* **1978,** *48*, 1-25.

11. Kalinowski, J.; Godlewski, J., Magnetic field effects on recombination radiation in tetracene crystal. *Chem. Phys. Lett.* **1975,** *36*, 345-348.

12. Geacintov, N. E.; Binder, M.; Swenberg, C. E.; Pope, M., Exciton dynamics in α-particle tracks in organic crystals: Magnetic field study of the scintillation in tetracene crystals. *Physical Review B* **1975,** *12*, 4113-4134.

13. Lohmann, F.; Mehl, W., Dark Injection and Radiative Recombination of Electrons and Holes in Naphthalene Crystals. *The Journal of Chemical Physics* **1969,** *50*, 500-506.

14. Hwang, W.; Kao, K. C., On the theory of filamentary double injection and electroluminescence in molecular crystals. *The Journal of Chemical Physics* **1974,** *60*, 3845-3855.

15. Bradley, L. L. T.; Schwob, H. P.; Weitz, D.; Williams, D. F., Delayed Electroluminescence Quenching in Anthracene. *Mol Cryst Liq Cryst* **1973,** *23*, 271-282.

16. Roberts, G.; McGinnity, M.; Barlow, W.; Vincett, P., Electroluminescence, photoluminescence and electroabsorption of a lightly substituted anthracene Langmuir film. *Solid State Commun.* **1979,** *32*, 683-686.

17. Roberts, G.; Keating, B.; Vincett, P.; Barlow, W., Electroabsorption in disordered solids. II. Anthracene crystals and thin films. *Journal of Physics C: Solid State Physics* **1978,** *11*, 3847.

18. Vincett, P.; Barlow, W.; Hann, R.; Roberts, G., Electrical conduction and low voltage blue electroluminescence in vacuum-deposited organic films. *Thin Solid Films* **1982,** *94*, 171-183.

19. Burgess, R. M.; Gouterman, M.; Khalil, G. E., Novel ultraviolet electroluminescence from Al/octaethylporphyrin/Ag film sandwich cells. *J. Lumin.* **1983,** *28*, 377-384.

20. Sinha, N.; Misra, Y.; Tripathi, L.; Misra, M., Electro-optical properties of doped anthracene films. *Solid State Commun.* **1981,** *39*, 89-91.

21. Partridge, R. H., Electro-Luminescence from Polyvinylcarbazole Films .1. Carbazole Cations. *Polymer* **1983,** *24*, 733-738.

22. Partridge, R. H., Electro-Luminescence from Polyvinylcarbazole Films .2. Polyvinylcarbazole Films Containing Antimony Pentachloride. *Polymer* **1983,** *24*, 739-747.

23. Partridge, R. H., Electro-Luminescence from Polyvinylcarbazole Films .3. Electroluminescent Devices. *Polymer* **1983,** *24*, 748-754.

24. Partridge, R. H., Electro-Luminescence from Polyvinylcarbazole Films .4. Electro-Luminescence Using Higher Work Function Cathodes. *Polymer* **1983,** *24*, 755-762.

25. Hayashi, S.; Etoh, H.; Saito, S., Electroluminescence of Perylene Films with a Conducting Polymer as an Anode. *Jpn J Appl Phys 2* **1986,** *25*, 773-775.

26. Tang, C.; VanSlyke, S., Organic electroluminescent diodes. *Appl. Phys. Lett.* **1987,** *51*, 913-916.

27. Adachi, C.; Tokito, S.; Tsutsui, T.; Saito, S., ELECTROLUMINESCENCE IN ORGANIC FILMS WITH 3-LAYER STRUCTURE. *Jpn J Appl Phys 2* **1988,** *27*, 269-271.

28. Burroughes, J. H.; Bradley, D. D. C.; Brown, A. R.; Marks, R. N.; Mackay, K.; Friend, R. H.; Burns, P. L.; Holmes, A. B., Light-Emitting-Diodes Based on Conjugated Polymers. *Nature* **1990,** *347*, 539-541.

29. Baldo, M. A.; O'Brien, D. F.; You, Y.; Shoustikov, A.; Sibley, S.; Thompson, M. E.; Forrest, S. R., Highly efficient phosphorescent emission from organic electroluminescent devices. *Nature* **1998,** *395*, 151-154.

30. Adachi, C.; Baldo, M. A.; Thompson, M. E.; Forrest, S. R., Nearly 100% internal phosphorescence efficiency in an organic light-emitting device. *J. Appl. Phys.* **2001,** *90*, 5048-5051.

31. Blochwitz, J.; Pfeiffer, M.; Fritz, T.; Leo, K., Low voltage organic light emitting diodes featuring doped phthalocyanine as hole transport material. *Appl. Phys. Lett.* **1998,** *73*, 729-731.

32. He, G. F.; Schneider, O.; Qin, D. S.; Zhou, X.; Pfeiffer, M.; Leo, K., Very high-efficiency and low voltage phosphorescent organic light-emitting diodes based on a p-i-n junction. *J. Appl. Phys.* **2004,** *95*, 5773-5777.

33. Geffroy, B.; le Roy, P.; Prat, C., Organic light-emitting diode (OLED) technology: materials, devices and display technologies. *Polym. Int.* **2006,** *55*, 572-582.

34. Hung, L. S.; Tang, C. W.; Mason, M. G., Enhanced electron injection in organic electroluminescence devices using an Al/LiF electrode. *Appl. Phys. Lett.* **1997,** *70*, 152-154.

35. Alan, J. H.; Yong, C.; Ian, D. P.; Gang, Y.; Chi, Z., Improved quantum efficiency for electroluminescence in semiconducting polymers. *Nature* **1999,** *397*, 414-417.

36. Shuai, Z.; Beljonne, D.; Silbey, R. J.; Bredas, J. L., Singlet and triplet exciton formation rates in conjugated polymer light-emitting diodes. *Phys. Rev. Lett.* **2000,** *84*, 131-134.

37. Baldo, M.; Lamansky, S.; Burrows, P., Very high-efficiency green organic light-emitting devices based on electrophosphorescence. *Appl. Phys. Lett.* **1999,** *75*, 4-6.

38. Adachi, C.; Baldo, M. A.; Forrest, S. R., Electroluminescence mechanisms in organic light emitting devices employing a europium chelate doped in a wide energy gap bipolar conducting host. *J. Appl. Phys.* **2000,** *87*, 8049-8055.

39. Adachi, C.; Baldo, M. A.; Forrest, S. R.; Thompson, M. E., High-efficiency organic electrophosphorescent devices with tris(2-phenylpyridine)iridium doped into electron-transporting materials. *Appl. Phys. Lett.* **2000,** *77*, 904-906.

40. Baldo, M.; Thompson, M.; Forrest, S., High-efficiency fluorescent organic light-emitting devices using a phosphorescent sensitizer. *Nature* **2000,** *403*, 750-753.

41. Shi, J. M.; Tang, C. W., Doped organic electroluminescent devices with improved stability. *Appl. Phys. Lett.* **1997,** *70*, 1665-1667.

42. Martens, J. H. F.; Marseglia, E. A.; Bradley, D. D. C.; Friend, R. H.; Burn, P. L.; Holmes, A. B., The Effect of Side-Groups on the Structure and Ordering of Poly(P-Phenylene Vinylene) Derivatives. *Synth. Met.* **1993,** *55*, 449-453.

43. Gustafsson, G.; Cao, Y.; Treacy, G. M.; Klavetter, F.; Colaneri, N.; Heeger, A. J., Flexible Light-Emitting-Diodes Made from Soluble Conducting Polymers. *Nature* **1992,** *357*, 477-479.

44. Mccullough, R. D.; Lowe, R. D.; Jayaraman, M.; Anderson, D. L., Design, Synthesis, and Control of Conducting Polymer Architectures - Structurally Homogeneous Poly(3-Alkylthiophenes). *J. Org. Chem.* **1993,** *58*, 904-912.

45. Mccullough, R. D.; Lowe, R. D., Enhanced Electrical-Conductivity in Regioselectively Synthesized Poly(3-Alkylthiophenes). *J Chem Soc Chem Comm* **1992**, 70-72.

46. Beljonne, D.; Ye, A.; Shuai, Z.; Brédas, J. L., Chain-Length Dependence of Singlet and Triplet Exciton Formation Rates in Organic Light-Emitting Diodes. *Adv. Funct. Mater.* **2004,** *14*, 684-692.

47. Dhoot, A. S.; Ginger, D. S.; Beljonne, D.; Shuai, Z.; Greenham, N. C., Triplet formation and decay in conjugated polymer devices. *Chem. Phys. Lett.* **2002,** *360*, 195-201.

48. Yin, S. W.; Chen, L. P.; Xuan, P. F.; Chen, K. Q.; Shuai, Z., Field effect on the singlet and triplet exciton formation in organic/polymeric light-emitting diodes. *J. Phys. Chem. B* **2004,** *108*, 9608-9613.

49. Wilson, J. S.; Dhoot, A. S.; Seeley, A. J. A. B.; Khan, M. S.; Kohler, A.; Friend, R. H., Spin-dependent exciton formation in pi-conjugated compounds. *Nature* **2001,** *413*, 828-831.

50. Wohlgenannt, M.; Tandon, K.; Mazumdar, S.; Ramasesha, S.; Vardeny, Z. V., Formation cross-sections of singlet and triplet excitons in pi-conjugated polymers. *Nature* **2001,** *409*, 494-497.

51. Wohlgenannt, M.; Jiang, X. M.; Vardeny, Z. V.; Janssen, R. A. J., Conjugation-length dependence of spin-dependent exciton formation rates in π-conjugated oligomers and polymers. *Phys. Rev. Lett.* **2002,** *88*, 197401.

52. Segal, M.; Baldo, M.; Holmes, R.; Forrest, S.; Soos, Z., Excitonic singlet-triplet ratios in molecular and polymeric organic materials. *Physical Review B* **2003,** *68*, 75211.

53. Reufer, M.; Walter, M. J.; Lagoudakis, P. G.; Hummel, B.; Kolb, J. S.; Roskos, H. G.; Scherf, U.; Lupton, J. M., Spin-conserving carrier recombination in conjugated polymers. *Nature Materials* **2005,** *4*, 340-346.

54. Zhen, C. G.; Chen, Z. K.; Liu, Q. D.; Dai, Y. F.; Shin, R. Y. C.; Chang, S. Y.; Kieffer, J., Fluorene-Based Oligomers for Highly Efficient and Stable Organic Blue-Light-Emitting Diodes. *Adv. Mater.* **2009,** *21*, 2425-2429.

55. Gorman, C., Metallodendrimers: Structural diversity and functional behavior. *Adv. Mater.* **1998,** *10*, 295-309.

56. Bosman, A. W.; Janssen, H. M.; Meijer, E. W., About Dendrimers: Structure, Physical Properties, and Applications. *Chem. Rev.* **1999,** *99*, 1665-1688.

57. Halim, M.; Pillow, J. N. G.; Samuel, I. D. W.; Burn, P. L., Conjugated dendrimers for light-emitting diodes: Effect of generation. *Adv. Mater.* **1999,** *11*, 371-374.

58. Halim, M.; Samuel, I. D. W.; Pillow, J. N. G.; Burn, P. L., Conjugated dendrimers for LEDs: Control of colour. *Synth. Met.* **1999,** *102*, 1113-1114.

59. Halim, M.; Samuel, I. D. W.; Pillow, J. N. G.; Monkman, A. P.; Burn, P. L., Control of colour and charge injection in conjugated dendrimer polypyridine bilayer LEDs. *Synth. Met.* **1999,** *102*, 1571-1574.

60. Newkome, G. R.; He, E. F.; Moorefield, C. N., Suprasupermolecules with novel properties: Metallodendrimers. *Chem. Rev.* **1999,** *99*, 1689-1746.

61. Pillow, J. N. G.; Burn, P. L.; Samuel, I. D. W.; Halim, M., Synthetic routes to phenylene vinylene dendrimers. *Synth. Met.* **1999,** *102*, 1468-1469.

62. Adronov, A.; Fréchet, J. M. J., Light-harvesting dendrimers. *Chem. Commun.* **2000**, 1701-1710.

63. Grayson, S. M.; Fréchet, J. M. J., Convergent dendrons and dendrimers: from synthesis to applications. *Chem. Rev.* **2001,** *101*, 3819-3867.

64. Tully, D. C.; Fréchet, J. M. J., Dendrimers at surfaces and interfaces: chemistry and applications. *Chem. Commun.* **2001**, 1229-1239.

65. Holder, E.; Langeveld, B. M. W.; Schubert, U. S., New trends in the use of transition metal-ligand complexes for applications in electroluminescent devices. *Adv. Mater.* **2005,** *17*, 1109-1121.

66. Wang, P. W.; Liu, Y. J.; Devadoss, C.; Bharathi, P.; Moore, J. S., Electroluminescent diodes from a single-component emitting layer of dendritic macromolecules. *Adv. Mater.* **1996,** *8*, 237-241.

67. Kwok, C. C.; Wong, M. S., Synthesis and Light-Emitting Properties of Difunctional Dendritic Distyrylstilbenes. *Macromolecules* **2001,** *34*, 6821-6830.

68. Freeman, A. W.; Koene, S. C.; Malenfant, P. R. L.; Thompson, M. E.; Fréchet, J. M. J., Dendrimer-Containing Light-Emitting Diodes: Toward Site-Isolation of Chromophores. *J. Am. Chem. Soc.* **2000,** *122*, 12385-12386.

69. Swallen, S. F.; Shi, Z.-Y.; Tan, W.; Xu, Z.; Moore, J. S.; Kopelman, R., Exciton localization hierarchy and directed energy transfer in conjugated linear aromatic chains and dendrimeric supermolecules. *J. Lumin.* **1998,** *76–77*, 193-196.

70. Bar-Haim, A.; Klafter, J., Dendrimers as light harvesting antennae. *J. Lumin.* **1998,** *76–77*, 197-200.

71. Lupton, J. M.; Samuel, I. D. W.; Beavington, R.; Burn, P. L.; Bassler, H., Control of charge transport and intermolecular interaction in organic light-emitting diodes by dendrimer generation. *Adv. Mater.* **2001,** *13*, 258-261.

72. Chiang, C. J.; Kimyonok, A.; Etherington, M. K.; Griffiths, G. C.; Jankus, V.; Turksoy, F.; Monkman, A. P., Ultrahigh Efficiency Fluorescent Single and Bi-Layer Organic Light Emitting Diodes: The Key Role of Triplet Fusion. *Adv. Funct. Mater.* **2013,** *23*, 739-746.

73. Hirohiko, F.; Takahisa, S.; Noriyuki, O.; Shizuo, T.; Katsumi, T.; Hideo, F., Anthracene derivatives as efficient emitting hosts for blue organic light-emitting diodes utilizing triplet–triplet annihilation. *Org. Electron.* **2012,** *13*, 1197-1203.

74. Kondakov, D. Y.; Pawlik, T. D.; Hatwar, T. K.; Spindler, J. P., Triplet annihilation exceeding spin statistical limit in highly efficient fluorescent organic light-emitting diodes. *J. Appl. Phys.* **2009,** *106*, 124510.

75. Zhen, C. G.; Dai, Y. F.; Zeng, W. J.; Ma, Z.; Chen, Z. K.; Kieffer, J., Achieving Highly Efficient Fluorescent Blue Organic Light-Emitting Diodes Through Optimizing Molecular Structures and Device Configuration. *Adv. Funct. Mater.* **2011,** *21*, 699-707.

76. Kondakov, D. Y., Role of triplet-triplet annihilation in highly efficient fluorescent devices. *Journal of the Society for Information Display* **2009,** *17*, 137-144.

77. Ganzorig, C.; Fujihira, M., A possible mechanism for enhanced electrofluorescence emission through triplet-triplet annihilation in organic electroluminescent devices. *Appl. Phys. Lett.* **2002,** *81*, 3137-3139.

78. Masui, K.; Nakanotani, H.; Adachi, C., Analysis of exciton annihilation in high-efficiency sky-blue organic light-emitting diodes with thermally activated delayed fluorescence. *Org. Electron.* **2013,** *14*, 2721-2726.

79. Popovic, Z. D.; Aziz, H., Delayed electroluminescence in small-molecule-based organic light-emitting diodes: Evidence for triplet-triplet annihilation and recombination-center-mediated light-generation mechanism. *J. Appl. Phys.* **2005,** *98*, 013510.

80. Luo, Y.; Aziz, H., Correlation Between Triplet–Triplet Annihilation and Electroluminescence Efficiency in Doped Fluorescent Organic Light-Emitting Devices. *Adv. Funct. Mater.* **2010,** *20*, 1285-1293.

81. Weichsel, C.; Burtone, L.; Reineke, S.; Hintschich, S. I.; Gather, M. C.; Leo, K.; Lussem, B., Storage of charge carriers on emitter molecules in organic light-emitting diodes. *Physical Review B* **2012,** *86*.

82. Yun, C. H.; Xie, G. H.; Murawski, C.; Lee, J.; Ventsch, F.; Leo, K.; Gather, M. C., Understanding the influence of doping in efficient phosphorescent organic light-emitting diodes with an organic p-i-n homojunction. *Org. Electron.* **2013,** *14*, 1695-1703.

83. Kondakov, D. Y., Characterization of triplet-triplet annihilation in organic light-emitting diodes based on anthracene derivatives. *J. Appl. Phys.* **2007,** *102*, 114504.

84. Luo, Y.; Aziz, H., Probing triplet-triplet annihilation zone and determining triplet exciton diffusion length by using delayed electroluminescence. *J. Appl. Phys.* **2010,** *107*, 094510.

85. Baldo, M. A.; Adachi, C.; Forrest, S. R., Transient analysis of organic electrophosphorescence. II. Transient analysis of triplet-triplet annihilation. *Physical Review B* **2000,** *62*, 10967-10977.

86. Yokoyama, D.; Park, Y.; Kim, B.; Kim, S.; Pu, Y. J.; Kido, J.; Park, J., Dual efficiency enhancement by delayed fluorescence and dipole orientation in high-efficiency fluorescent organic light-emitting diodes. *Appl. Phys. Lett.* **2011,** *99*, 123303.

87. Wallikewitz, B. H.; Kabra, D.; Gelinas, S.; Friend, R. H., Triplet dynamics in fluorescent polymer light-emitting diodes. *Physical Review B* **2012,** *85*.

88. Shao, M.; Yan, L.; Li, M.; Ilia, I.; Hu, B., Triplet-charge annihilation versus triplet-triplet annihilation in organic semiconductors. *Journal of Materials Chemistry C* **2013,** *1*, 1330-1336.

89. Song, D.; Zhao, S.; Luo, Y.; Aziz, H., Causes of efficiency roll-off in phosphorescent organic light emitting devices: Triplet-triplet annihilation versus triplet-polaron quenching. *Appl. Phys. Lett.* **2010,** *97*, 243304.

90. Yoan, C. S.; Christoph, W., Low-power photon upconversion through triplet–triplet annihilation in polymers. *J. Mater. Chem.* **2012,** *22*, 20817.

91. Hoffmann, S.; Koenen, J.-M.; Scherf, U.; Bauer, I.; Strohriegl, P.; Bässler, H.; Köhler, A., Triplet-triplet annihilation in a series of poly(p-phenylene) derivatives. *The journal of physical chemistry. B* **2011,** *115*, 8417-8423.

92. King, S. M.; Cass, M.; Pintani, M.; Coward, C.; Dias, F. B.; Monkman, A. P.; Roberts, M., The contribution of triplet--triplet annihilation to the lifetime and efficiency of fluorescent polymer organic light emitting diodes. *J. Appl. Phys.* **2011,** *109*, 074502.

93. Fukagawa, H.; Shimizu, T.; Ohbe, N.; Tokito, S.; Tokumaru, K.; Fujikake, H., Anthracene derivatives as efficient emitting hosts for blue organic light-emitting diodes utilizing triplet-triplet annihilation. *Org. Electron.* **2012,** *13*, 1197-1203.

94. Wu, S.; Aonuma, M.; Zhang, Q.; Huang, S.; Nakagawa, T.; Kuwabara, K.; Adachi, C., High-efficiency deep-blue organic light-emitting diodes based on a thermally activated delayed fluorescence emitter. *Journal of Materials Chemistry C* **2014,** *2*, 421-424.

95. Tanaka, H.; Shizu, K.; Nakanotani, H.; Adachi, C., Twisted Intramolecular Charge Transfer State for Long-Wavelength Thermally Activated Delayed Fluorescence. *Chem. Mater.* **2013,** *25*, 3766-3771.

96. Serevicius, T.; Nakagawa, T.; Kuo, M. C.; Cheng, S. H.; Wong, K. T.; Chang, C. H.; Kwong, R. C.; Xia, S.; Adachi, C., Enhanced electroluminescence based on thermally activated delayed fluorescence from a carbazole-triazine derivative. *Phys. Chem. Chem. Phys.* **2013,** *15*, 15850-15855.

97. Sato, K.; Shizu, K.; Yoshimura, K.; Kawada, A.; Miyazaki, H.; Adachi, C., Organic Luminescent Molecule with Energetically Equivalent Singlet and Triplet Excited States for Organic Light-Emitting Diodes. *Phys. Rev. Lett.* **2013,** *110*, 247401.

98. Nasu, K.; Nakagawa, T.; Nomura, H.; Lin, C. J.; Cheng, C. H.; Tseng, M. R.; Yasuda, T.; Adachi, C., A highly luminescent spiro-anthracenone-based organic light-emitting diode exhibiting thermally activated delayed fluorescence. *Chem. Commun.* **2013,** *49,* 10385-10387.

99. Nakanotani, H.; Masui, K.; Nishide, J.; Shibata, T.; Adachi, C., Promising operational stability of high-efficiency organic light-emitting diodes based on thermally activated delayed fluorescence. *Scientific reports* **2013,** *3,* 2127.

100. Li, J.; Nakagawa, T.; Macdonald, J.; Zhang, Q.; Nomura, H.; Miyazaki, H.; Adachi, C., Highly efficient organic light-emitting diode based on a hidden thermally activated delayed fluorescence channel in a heptazine derivative. *Adv. Mater.* **2013,** *25,* 3319-3323.

101. Lee, J.; Shizu, K.; Tanaka, H.; Nomura, H.; Yasuda, T.; Adachi, C., Oxadiazole- and triazole-based highly-efficient thermally activated delayed fluorescence emitters for organic light-emitting diodes. *Journal of Materials Chemistry C* **2013,** *1,* 4599-4604.

102. Jiyoung, L.; Katsuyuki, S.; Hiroyuki, T.; Hiroko, N.; Takuma, Y.; Chihaya, A., Oxadiazole- and triazole-based highly-efficient thermally activated delayed fluorescence emitters for organic light-emitting diodes. *Journal of Materials Chemistry C* **2013,** *1,* 4599.

103. Zhang, Q.; Li, J.; Shizu, K.; Huang, S.; Hirata, S.; Miyazaki, H.; Adachi, C., Design of efficient thermally activated delayed fluorescence materials for pure blue organic light emitting diodes. *J. Am. Chem. Soc.* **2012,** *134,* 14706-14709.

104. Uoyama, H.; Goushi, K.; Shizu, K.; Nomura, H.; Adachi, C., Highly efficient organic light-emitting diodes from delayed fluorescence. *Nature* **2012,** *492,* 234-238.

105. Tanaka, H.; Shizu, K.; Miyazaki, H.; Adachi, C., Efficient green thermally activated delayed fluorescence (TADF) from a phenoxazine-triphenyltriazine (PXZ-TRZ) derivative. *Chem. Commun.* **2012,** *48,* 11392-11394.

106. Nakagawa, T.; Ku, S. Y.; Wong, K. T.; Adachi, C., Electroluminescence based on thermally activated delayed fluorescence generated by a spirobifluorene donor-acceptor structure. *Chem. Commun.* **2012,** *48,* 9580-9582.

107. Méhes, G.; Nomura, H.; Zhang, Q.; Nakagawa, T.; Adachi, C., Enhanced electroluminescence efficiency in a spiro-acridine derivative through thermally activated delayed fluorescence. *Angewandte Chemie (International ed. in English)* **2012,** *51,* 11311-11315.

108. Lee, S. Y.; Yasuda, T.; Nomura, H.; Adachi, C., High-efficiency organic light-emitting diodes utilizing thermally activated delayed fluorescence from triazine-based donor--acceptor hybrid molecules. *Appl. Phys. Lett.* **2012,** *101,* 093306.

109. Endo, A.; Sato, K.; Yoshimura, K.; Kai, T.; Kawada, A.; Miyazaki, H.; Adachi, C., Efficient up-conversion of triplet excitons into a singlet state and its application for organic light emitting diodes. *Appl. Phys. Lett.* **2011,** *98,* 083302.

110. Julius, C. F.; Diana, R.; Joel, M. H., Delayed Fluorescence Optical Thermometry. *Anal. Chem.* **1995,** *67,* 4269-4275.

111. Filipa, A. S.; Aleksandre, F.; Mário, N. B.-S., A study of thermally activated delayed fluorescence in C60. *Chem. Phys. Lett.* **1997,** *271,* 361-366.

112. Bachilo, S. M.; Benedetto, A. F.; Weisman, R. B.; Nossal, J. R.; Billups, W. E., Time-resolved thermally activated delayed fluorescence in C-70 and 1,2-C70H2. *J. Phys. Chem. A* **2000,** *104,* 11265-11269.

113. Baleizao, C.; Berberan-Santos, M. N., Thermally activated delayed fluorescence in fullerenes. In *Fluorescence Methods and Applications: Spectroscopy, Imaging, and Probes,*2008; Vol. 1130, pp 224-234.

114. Czerwieniec, R.; Yu, J. B.; Yersin, H., Blue-Light Emission of Cu(I) Complexes and Singlet Harvesting. *Inorg. Chem.* **2011,** *50*, 8293-8301.

115. Endo, A.; Ogasawara, M.; Takahashi, A.; Yokoyama, D.; Kato, Y.; Adachi, C., Thermally activated delayed fluorescence from Sn(4+)-porphyrin complexes and their application to organic light emitting diodes--a novel mechanism for electroluminescence. *Adv. Mater.* **2009,** *21*, 4802-4806.

116. Goushi, K.; Yoshida, K.; Sato, K.; Adachi, C., Organic light-emitting diodes employing efficient reverse intersystem crossing for triplet-to-singlet state conversion. *Nature Photonics* **2012,** *6*, 253-258.

117. Berberan-Santos, M. N.; Garcia, J. M. M., Unusually Strong Delayed Fluorescence of C70. *J. Am. Chem. Soc.* **1996,** *118*, 9391-9394.

118. Baleizao, C.; Berberan-Santos, M. N., Thermally activated delayed fluorescence as a cycling process between excited singlet and triplet states: Application to the fullerenes. *The Journal of Chemical Physics* **2007,** *126*, 204510.

119. Park, S.; Kwon, O. H.; Lee, Y. S.; Jang, D. J.; Park, S. Y., Imidazole-based excited-state intramolecular proton-transfer(ESIPT) materials: Observation of thermally activated delayed fluorescence(TDF). *J. Phys. Chem. A* **2007,** *111*, 9649-9653.

120. Giacobbe, E. M.; Mi, Q. X.; Colvin, M. T.; Cohen, B.; Ramanan, C.; Scott, A. M.; Yeganeh, S.; Marks, T. J.; Ratner, M. A.; Wasielewski, M. R., Ultrafast Intersystem Crossing and Spin Dynamics of Photoexcited Perylene-3,4:9,10-bis(dicarboximide) Covalently Linked to a Nitroxide Radical at Fixed Distances. *J. Am. Chem. Soc.* **2009,** *131*, 3700-3712.

121. Paul, B. K.; Samanta, A.; Guchhait, N., Implication toward a Simple Strategy To Generate Efficiency-Tunable Fluorescence Resonance Energy Transfer Emission: Intertwining Medium-Polarity-Sensitive Intramolecular Charge Transfer Emission to Fluorescence Resonance Energy Transfer. *J. Phys. Chem. A* **2010,** *114*, 6097-6102.

122. Marian, C. M., Spin-orbit coupling and intersystem crossing in molecules. *Wiley Interdisciplinary Reviews-Computational Molecular Science* **2011,** *2*, 187-203.

Chapter 2

Color tunable thermally activated delayed fluorescence from bipolar molecules with 5-phenyl-5,10-dihydrophenazine as donor

2.1 Introduction

Currently, the design strategy of TADF molecules is based on the effective separation of the spatial distribution of the HOMO and LUMO. Until now, a various kinds of TADF molecules having charge-transfer (CT) characteristics based on a donor-acceptor structure were developed.[1-9] In particular, a phenoxazine–triphenyltriazine derivative (**PXZ**-**TRZ**) showed excellent OLED performance, demonstrating a maximum EQE of 12% with the emission peak at 529 nm.[1] A large dihedral angle between the donor and acceptor planes induced by steric repulsion suppressed the nonradiative decay process and facilitated the upconversion from triplet to singlet-excited states. In the optimization of the molecular structures, when we used 5-phenyl-5,10-dihydrophenazine (**PPZ**) as a donor instead of **PXZ**, I observed a significant decrease of EQE, resulted in only 1% with the large redshift of the emission peak into 600 nm. However, it is rather hard to conclude that **PPZ** is not a useful donor unit for the construction of efficient TADF emitters. An elucidation of this low efficiency will help me understand the key factors affecting the photoluminescence (PL) quantum yield (PLQY) of CT molecules and pave the way for TADF molecular design. A series of D-A type molecules with **PPZ** as a donor are designed and synthesized in this study. Their decay constants derived from lifetimes and PLQYs are discussed with their structures.

2.2 Molecular structure and calculated results

The molecules used in this work are shown in Fig. 2-1. All D-A-type molecules of **PPZ**-**TRZ**, **PPZ**-**DPO**, **PPZ**-**3TPT** and **PPZ**-**4TPT** have a **PPZ** donor unit, while the different acceptor units of 1,3,5-triazine (**TRZ**), 2,5-diphenyl-1,3,4-oxadiazole (**DPO**) and 3,4,5-triphenyl-1,2,4-triazole (**TPT**) were used. These **PPZ** derivatives were synthesized following the procedure described below.
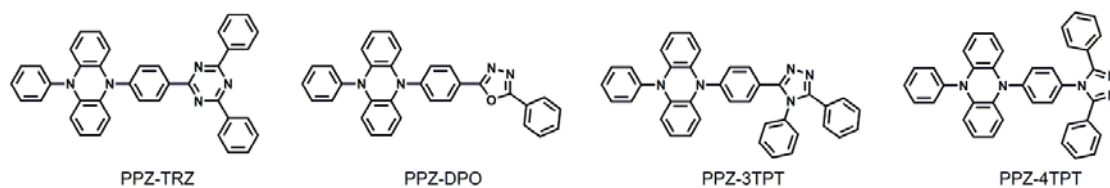
24

Figure 2-1. Chemical structures of **PPZ-TRZ**, **PPZ-DPO**, **PPZ-3TPT** and **PPZ-4TPT**.

Table 2-1. Gaussian calculation results of **PPZ-TRZ**, **PPZ-DPO**, **PPZ-3TPT** and **PPZ-4TPT**.

	HOMO	LUMO	S_1 (eV)	T_1 (eV)	ΔE_{ST} (eV)
PPZ-TRZ			1.6716	1.6667	0.0049
PPZ-DPO			1.9128	1.9025	0.0103
PPZ-3TPT			2.3443	2.3321	0.0122
PPZ-4TPT			2.5436	2.4805	0.0631

We used density functional theory (DFT) with the most popular functional, B3LYP, to simulate the ground-state geometries of these four compounds.[10] B3LYP applies Becke's three-parameter exchange functional (B3) in combination with Lee, Yang, and Parr's correlation functional (LYP) and Pople's 6-31G(d,p) basis set. The ten lowest singlet and triplet excited states were calculated by the time-dependent

density functional theory (TD-DFT) method at their optimized ground-state geometries using the same functional and basis set. These calculations were performed using Gaussian 09 package.[11] It has been employed successfully to determine the energetics and electron spin resonance (ESR) parameters for the neutral base radicals to a high degree of accuracy. The results are shown in Table 2-1.

Based on the quantum calculation results, I estimate that the dihedral angles between the donor and acceptor planes are almost vertical, leading to significant separation of their HOMOs and LUMOs as well as small singlet/triplet splitting of the involved transitions (Table 2-1). The distributions of the HOMOs are localized on **PPZ** units, while the LUMOs are localized on the acceptor units of **TRZ**, **DPO** and **TPT**. The ΔE_{ST} of all four **PPZ** compounds are estimated to be less than 0.1 eV. As shown in Table 2-1, the transition energies of S_1 are increased in the order of **PPZ-TRZ**, **PPZ-DPO**, **PPZ-3TPT** and **PPZ-4TPT**, indicating a blue-shift of the emission band with the same order.

2.3 Photophysical characteristics

The low-lying energy levels and photophysical properties of **PPZ-TRZ**, **PPZ-DPO**, **PPZ-3TPT** and **PPZ-4TPT** were investigated in toluene. Toluene is low polar aromatic solvent that provides similar environment for emitters as in an organic semiconductor film. As shown in Fig. 2-2, two absorption peaks can be observed in the solutions of **PPZ-TRZ**, **PPZ-DPO** and **PPZ-3TRZ** in which the lower ones can be ascribed to CT absorption while the higher ones are induced by local electron transition. The electron-withdrawing ability of the acceptors of **TRZ**, **DPO**, **3TPT** and **4TPT** decreases in this order. As a result, the CT absorption peaks of these compounds showed a blue shift subsequently. Conversely, the energy of the $^3\pi{-}\pi^*$ transition centered on the **PPZ** moiety is almost constant. For **PPZ-4TPT**, the CT

transfer energy is nearly the same as the locally excited (LE) state energy. As shown in Fig. 2-2, in toluene at room temperature, all compounds showed a broad and unstructured PL spectrum that can be ascribed to a CT transition. In toluene at 77K, the phosphorescent spectra (measured after 10 ms delay) of **PPZ-DPO**, **PPZ-3TRZ** and **PPZ-4TRZ** show well defined vibronic structures, indicating that their lowest triplet states are LE states. On the contrary, the broad and structureless phosphorescent band indicates a CT characteristic of the T_1 state of **PPZ-TRZ**.
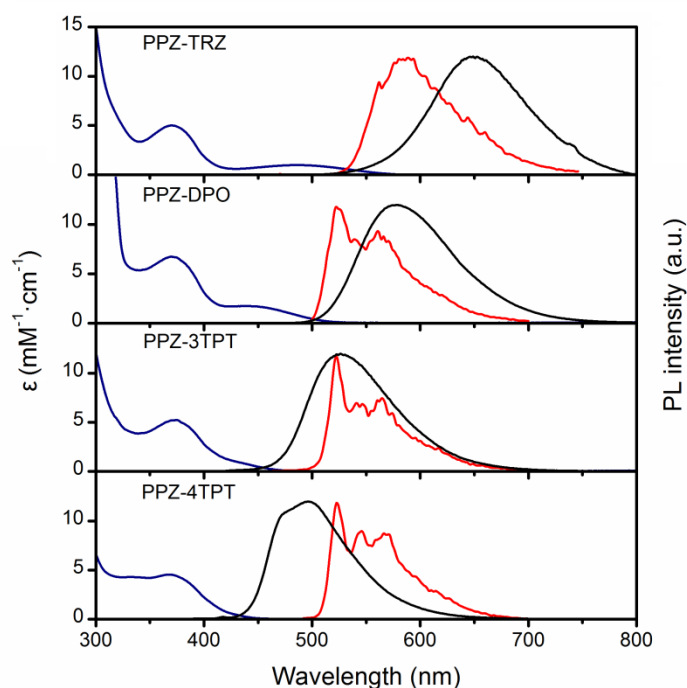
Figure 2-2. Absorption spectra of the TADF emitters in toluene at RT (blue line) and their fluorescence (black line) and phosphorescence (red line) spectra in toluene at RT and 77K, respectively.

The zero-zero energy of CT transitions were derived from the onsets of the emission bands, while that of the LE states were determined from the highest energy peaks of the spectra with vibronic structures. The ΔE_{ST} of **PPZ-DPO**, **PPZ-3TPT** and **PPZ-4TPT** in toluene at RT are calculated to be 0.05, 0.26 and 0.41 eV, respectively.

27

Although we cannot obtain the ΔE_{ST} of **PPZ-TRZ** by this way due to the redshift of the CT band in toluene glass at 77 K, a small ΔE_{ST} can be expected in **PPZ-TRZ** because of the small energy difference between ^{1}CT and ^{3}CT as predicted by TD-DFT. The experimental energy levels of ^{1}CT and ^{3}LE states combined with the calculated energy levels of ^{3}CT states for these four compounds are summarized in Fig. 2-3.
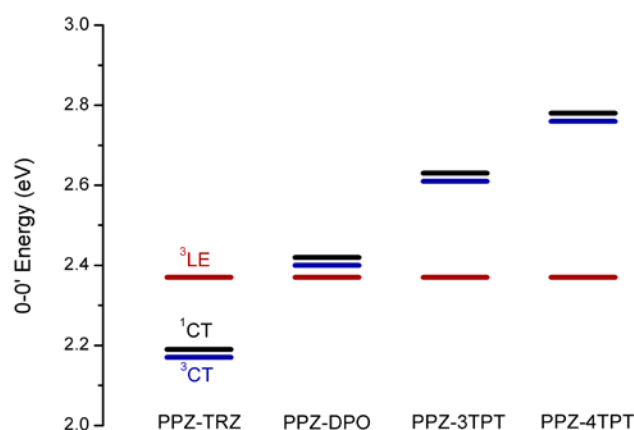

Figure 2-3. The excited state energies of ^{1}CT, ^{3}CT and ^{3}LE states. The 0-0´ energies of ^{1}CT state are determined from the fluorescence spectra in toluene at RT, while that of the ^{3}LE state localized over the **PPZ** moieties is determined from the phosphorescence spectra in toluene at 77 K (Fig. 2-2). The energy differences between ^{1}CT and ^{3}CT states are derived from the computational prediction (Table 2-1).

In oxygen-free toluene at RT, the PLQY of 0.12 for **PPZ-DPO** are relatively higher than that of 0.01 for **PPZ-TRZ**, probably owing to the energy gap law. Although the emission energies of **PPZ-3TPT** and **PPZ-4TPT** are even higher than that of **PPZ-DPO**, their low-lying ^{3}LE states prevent efficient repopulation of the emissive ^{1}CT state. Instead, the energy from ^{3}LE states dissipates by non-radiative processes, leading to a low PLQY of 0.07 for **PPZ-3TPT** and 0.04 for **PPZ-4TPT** in toluene. In oxygen-free toluene at RT, the delayed components can be clearly observed from **PPZ-DPO** and **PPZ-3TPT**, while the long-lived excited states in

PPZ-**4TPT** and **PPZ**-**TRZ** are completely quenched by nonradiative decay in the fluid solution.

The photophysical properties of these molecules were also investigated in 10 wt%-doped **mCP** films. Fig. 2-4 shows the PL spectra of these doped films. Comparing with their emission spectra in toluene, we observed different degrees of blue shift for these compounds in **mCP** doped films. This can be explained by larger excited-state relaxation in fluid solutions.
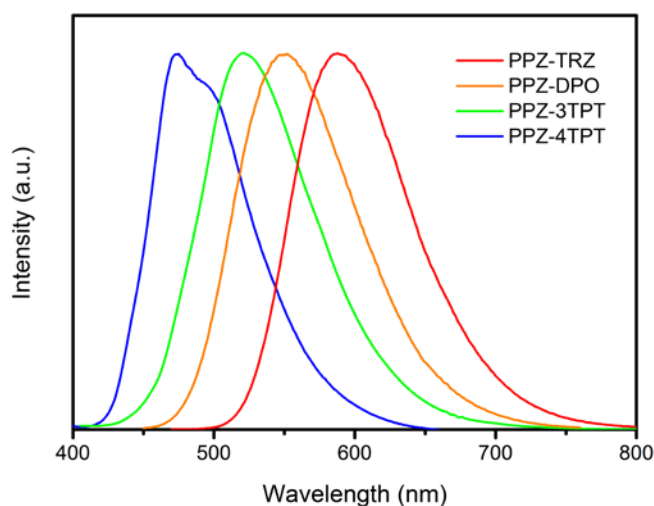

Figure 2-4. PL spectra of **PPZ**-**TRZ**, **PPZ**-**DPO**, **PPZ**-**3TPT** and **PPZ**-**4TPT** doped into **mCP** films (10 wt%).

The small ΔE_{ST} of **PPZ**-**TRZ** and **PPZ**-**DPO** ensures a short TADF lifetime (τ_{TADF}) of 0.14 μs and 3.6 μs for their doped films at room temperature (RT) along with a fluorescence lifetime (τ_F) of ns order (Fig. 2-5). Although ΔE_{ST} values are large for **PPZ**-**3TPT** and **PPZ**-**4TPT** in the doped films, TADF emission can also be observed with τ_{TADF} of 1.4 ms and 8.8 ms, respectively (Fig. 2-5).
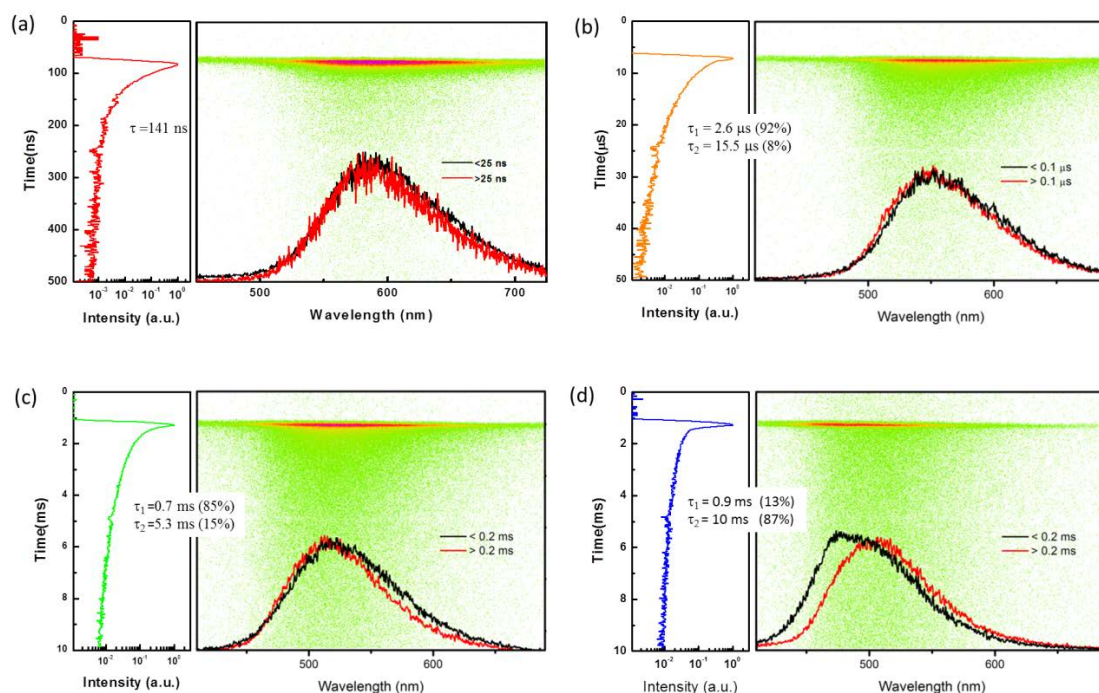
Figure 2-5. Streak image of the **mCP** films doped with 10 wt% of (a) **PPZ-TRZ**, (b) **PPZ-DPO**, (c) **PPZ-3TPT** and (d) **PPZ-4TPT**. The emission decays of the TADF components were fitted with a single exponential for **PPZ-TRZ** while two exponentials for other three compounds.

The photophysical data of the compounds in toluene and **mCP** films at RT is summarized in Table 2-1. We can find that the fluorescence rate (k_F) of each compound in solution and a doped film is comparable. However, the non-radiative rates (k_{IC})[1] in solid films are much lower than those in solution because a rigid matrix suppresses collision-induced intramolecular radiationless transitions and bimolecular processes. As a result, the PLQY values of **PPZ-TRZ**, **PPZ-DPO**, **PPZ-3TPT** and **PPZ-4TPT** were dramatically increased, resulted in 0.12, 0.45, 0.42 and 0.12, respectively, in the **mCP** films at room temperature.

---

[1] k_{IC} is internal conversion between S_1 and S_0 states and is given by the formula $\Phi = k_F /(k_F + k_{IC})$.

Table 2-2. Photophysical data of **PPZ** derivatives in toluene and **mCP** films at room temperature.

Parameter	PPZ-TRZ	PPZ-DPO	PPZ-3TPT	PPZ-4TPT
in toluene (0.1 mM)				
$\lambda_{max,em}$ (nm)	650	577	528	495
Φ_F	0.01	0.08	0.04	0.04
Φ_{TADF}	–	0.04	0.03	–
τ_F (ns)	2.2	9.0	3.9	3.6
τ_{TADF} (μs)	–	0.52	33	–
k_F ($\times 10^7$ s^{-1})	0.5	0.9	1.0	0.8
$k_{IC}{}^2$ ($\times 10^7$ s^{-1})	50	6.6	–	–
in mCP film (10 wt%)				
$\lambda_{max,em}$ (nm)	590	550	520	474
Φ_F	0.11	0.12	0.06	0.04
Φ_{TADF}	0.01	0.33	0.36	0.08
τ_F (ns)	7.2	7.0	3.5	2.8
$\tau_{TADF,AV}$ (μs)	0.14	3.6	1.4×10^3	8.8×10^3
k_F ($\times 10^7$ s^{-1})	1.5	1.7	1.7	1.4
k_{IC} ($\times 10^7$ s^{-1})	11	2.8	–	–

2.4 Device performance

OLED devices are fabricated to investigate the EL properties of these compounds. Fig. 2-6 displays the device configuration and chemical structures of molecules used in this experiment. A structure of **ITO**/**α-NPD** (40 nm)/**TADF**:**CBP** (6 wt%, 30 nm)/**TPBI**(60 nm)/LiF (0.5 nm)/Al (100 nm) is employed for **PPZ-TRZ**, **PPZ-DPO** and **PPZ-3TPT**. For **PPZ-4TPT**, a more complex device structure of **ITO**/**α-NPD** (30 nm)/**TCTA** (20 nm)/**CzSi** (10 nm)/**PPZ-4TRZ**:**DPEPO** (10 wt%, 20

---

[2] In the case of PPZ-3TPT and PPZ-4TPT, k_{IC} cann't be calculated using $\Phi = k_F /(k_F + k_{IC})$ for their relatively large ΔE_{ST}.

nm)/**DPEPO** (10 nm)/**TPBI** (30 nm)/LiF (0.5 nm)/Al (100 nm) is employed to get efficient carriers injection and transport.
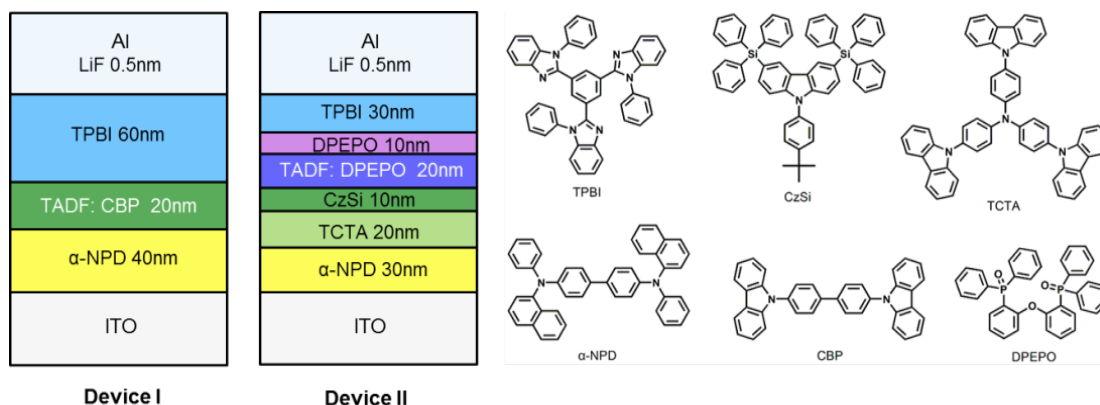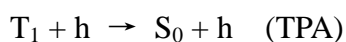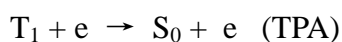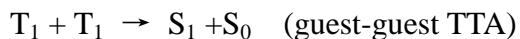

Figure 2-6. Device configuration and chemical structures of molecules utilized in this experiment; **PPZ-TRZ**, **PPZ-DPO** and **PPZ-3TPT** were tested in device I, **PPZ-4TPT** was tested in device II.

Fig. 2-7 demonstrates external quantum efficiency-current density characteristics (a), luminance-voltage characteristics (b), current density-voltage characteristics (c) and EL spectra (d) of the devices based on **PPZ-TRZ**, **PPZ-DPO**, **PPZ-3TPT** and **PPZ-4TPT**. Among these devices, **PPZ-DPO** and **PPZ-3TPT** based OLEDs showed the highest EQE because of their relatively high PLQY. However, a **PPZ-3TPT** based OLED showed significant roll-off at high current density. The well-known efficiency roll-off behavior in phosphorescence based OLEDs (PHOLEDs) is primarily attributed to the quenching mechanisms of triplet-triplet annihilation (TTA)[12] and triplet-polaron annihilation (TPA)[13] which can generally be described by the following schemes,

$T_1 + T_1 \rightarrow S_1 + S_0$ (guest-guest TTA)

$T_1 + T_1 \rightarrow T_1 + S_0$ (guest-guest TTA)

$T_1 + e \rightarrow S_0 + e$ (TPA)

$T_1 + h \rightarrow S_0 + h$ (TPA)

where T_1, S_1, S_0, e and h denote triplet exciton, singlet exciton, ground state, electron and hole polarons, respectively. Studies on these two mechanisms in PHOLEDs have been extensively reported, while different dominant mechanisms were also derived by different groups based on different devices.[12-17] As singlet exciton and triplet exciton coexist in TADF based OLEDs, K. Masui et al. recently proposed that the singlet–triplet annihilation (STA), i.e.,

$$T_1 + S_1 \rightarrow T_1 + S_0 \quad \text{(guest-guest STA)}$$

also dominate the efficiency roll-off, in addition to TTA and TPA processes.[18] Although it is difficult to quantitatively differentiate these three triplet quenching factors in TADF based OLEDs, the extra-long TADF lifetime of **PPZ**-**3TPT** should be responsible for the rapid EQE roll-off of its device. Similar EL characteristics were also observed in **PPZ**-**4TPT**, whose lifetime in a doped film is even longer than that of **PPZ**-**3TPT**. For **PPZ**-**TRZ** and **PPZ**-**DPO** based OLEDs, the roll-off is suppressed because of the shorter TADF lifetimes. However, **PPZ**-**TRZ** device showed a rather low EQE due to its large nonradiative decay rate governed by the energy gap law.
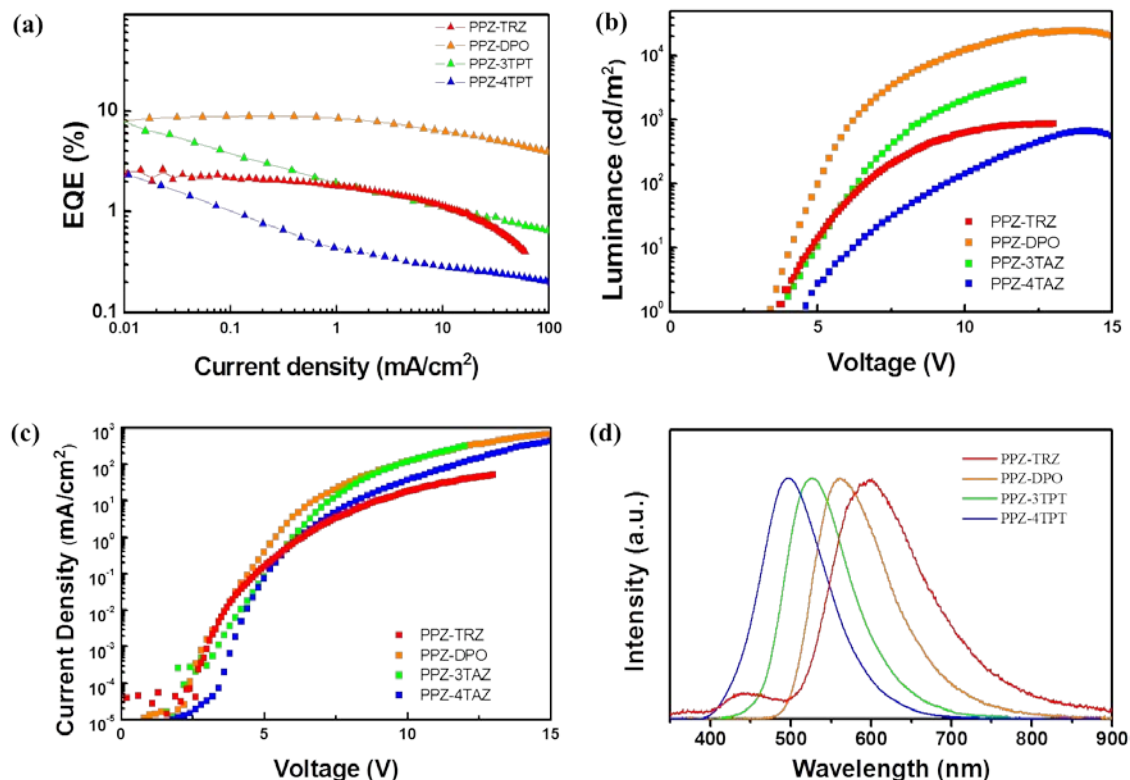
Figure 2-7. EQE versus current density (a), luminance versus voltage (b), current density versus voltage (c) and EL spectra (d) of **PPZ-DPO**, **PPZ-3TPT**, **PPZ-4TPT** and **PPZ-TRZ**.

2.5 Conclusion

In this chapter, we demonstrated a series of D-A type TADF molecules that have the same donor of **PPZ** with different acceptor unities. By adjusting the electron withdrawing abilities of the acceptor units, the emission peaks of TADF molecules can be tuned from 600 nm to 496 nm. We found that the blue shift of the emission peak energy decreases the nonradiative decay rate from a S_1 state, leading to higher PLQY. Yellow emitting **PPZ-DPO** demonstrated a relatively high PLQY of 0.45 in a 10 wt%-doped **mCP** film and a high maximum EQE of 9% in an OLED. Further enhancement of the CT-state energy will enlarge the energy difference between the lowest singlet ^{1}CT state and triplet $^3\pi$-π^* excited-state which is localized on a **PPZ** unit, respectively. The inefficient energy upconversion from the T_1 to S_1 states in the

34

green and sky-blue emitting **PPZ** derivatives, **PPZ-3TRZ** and **PPZ-4TRZ**, resulted in relatively low PLQYs as well as very long TADF lifetimes. For the OLEDs based on **PPZ-3TRZ** and **PPZ-4TRZ**, the extra-long lifetimes of these TADF emitters induced serious efficiency roll-off at high current density. The systematic studies in this chapter revealed that bipolar compounds with large twisting angle could emit efficient and short-lifetime of TADF only when the emission peak energy is high enough and the ^{3}LE state is close to or higher than the ^{3}CT state.

2.6 Experimental section

Quantum chemical calculations

All calculations were performed using the Gaussian 09 program package. The geometries in the ground state were optimized via DFT calculations at the B3LYP/6-31G* level. Vertical absorption energies (E_{vA}) were calculated based on TD-DFT with the B3LYP function using 6-31G* basis sets. The calculated $E_{vA}(S_1)$ corresponding to LE or CT transitions were distinguished by orbital transition analyses.

Synthesis

Reagents and anhydrous solvents were purchased from commercial sources and used as received. The starting materials 1,4-dichloro-1,4-bisphenyl- 2,3-diaza-1,3-butadiene,[19] 5-phenyl-5,10-dihydrophenazine,[20] 2-(4-bromo-phenyl)- 5-phenyl-1,3,4 -oxadiazole,[21] 3-(4-bromophenyl)-4.5-diphenyl-1,2,4-triazole[22] and 9,9-dimethyl-9,10-dihydroacridine[23] were prepared following literature procedures. ^{1}H nuclear magnetic resonance (NMR) and ^{13}C NMR spectra were recorded in DMSO-d_6 with a Bruker Avance 500 spectrometer (Germany) operating at 500 MHz for ^{1}H NMR and 125 MHz for ^{13}C NMR. Chemical shifts (δ) are given in parts per million (ppm)

relative to tetramethylsilane (TMS; $\delta = 0$) as the internal reference. ^{1}H NMR spectra data are reported as chemical shift, relative integral, multiplicity (s = singlet, d = doublet, t = triplet, m = multiplet), coupling constant (J in Hz) and assignment. Mass spectra were measured in positive ion atmospheric pressure chemical ionization (APCI) mode on a Waters 3100 mass detector. Elemental analyses (C, H, N) were carried out with a Yanaco MT-5 CHN corder.

4-(4-bromophenyl)-3,5-diphenyl-1,2,4-triazole:1,4-Dichloro-1,4-bisphenyl-2,3-diaza-1,3-butadiene (4.5 g, 16 mmol), 4-bromoaniline (2.0 g, 16 mmol) and N,N-dimethylaniline (30 mL) were added into a 100-mL three-necked flask. After the mixture was stirred for 5 h at 135℃ under nitrogen atmosphere, it was poured into 1M hydrochloric acid solution (100 mL) and stirred for another 0.5 h. The precipitate was collected by filtration and then dissolved in toluene. The organic layer was washed with saturated sodium carbonate solution and then dried over anhydrous magnesium sulfate. After evaporation of the solvent, the crude product was recrystallized from ethanol and hexane to obtain a white powder (2.3 g, 38%). ^{1}H NMR (DMSO-d_6, 500 MHz): δ [ppm] 7.67 (d, J = 8.5 Hz, 2H), 7.43–7.38 (m, 12H). ^{13}C NMR (DMSO-d_6, 125 MHz): δ [ppm] 154.2, 134.2, 132.7, 130.5, 129.7, 128.6, 128.5, 126.8, 122.9. APCI-MS m/z: 376 [M+1]$^+$. Anal. calcd for $C_{20}H_{14}BrN_3$: C, 63.84; H, 3.75; N, 11.17. Found: C, 63.97; H, 3.71; N, 11.19.

2-[4-(5-phenyl-5,10-dihydrophenazine)phenyl]-5-phenyl-1,3,4-oxadiazole (PPZ-DPO) : A toluene solution of freshly prepared 5-phenyl-5,10-dihydrophenazine (10 mL, ca. 6 mmol) and tri(*tert*-butyl)phosphine toluene (0.63 mL, 2 mol/L) was added to a 100-mL three-necked flask containing 2-(4-bromophenyl)-5-phenyl-1,3,4-oxadiazole (1.50 g, 5 mmol), palladium acetate (0.056 g, 0.25 mmol), potassium carbonate (1.84 g, 13.3 mmol), and toluene (10 mL) under nitrogen protection. The mixture was stirred for 10 h at 80℃ under nitrogen atmosphere. Water (10 mL) and chloroform (100 mL) were then added under stirring. The organic layer was separated

and dried with anhydrous magnesium sulfate. After filtration and evaporation of solvent, the residue was purified by column chromatography on silica gel (toluene: ethyl acetate = 4:1), giving the desired compound as a yellow powder (1.95 g, 82%). ^{1}H NMR (DMSO-d_6, 500 MHz): δ [ppm] 8.42 (d, J = 8.5 Hz, 2H), 8.18 (d, J = 8.0 Hz, 2H), 7.72–7.66 (m, 7H), 7.55 (t, J = 7.5 Hz, 1H), 7.43 (d, J = 8.5 Hz, 2H), 6.36–6.32 (m, 4H), 5.69 (d, J = 9.0 Hz, 2H), 5.58 (d, J = 9.0 Hz, 2H). ^{13}C NMR (DMSO-d_6, 125 MHz): δ [ppm] 164.2, 163.6, 143.4, 139.4, 136.3, 135.2, 132.1, 131.6, 131.5, 130.8, 130.0, 129.5, 128.5, 126.7, 123.3, 122.9, 121.5, 121.0, 113.0, 112.5. APCI-MS m/z: 478 [M+1]$^{+}$. Anal. calcd for $C_{32}H_{22}N_4O$: C, 80.32; H, 4.63; N, 11.71. Found: C, 80.45; H, 4.59; N, 11.63.

3-[4-(5-phenyl-5,10-dihydrophenazine)phenyl]-4,5-diphenyl-1,2,4-triazole (PPZ -3TPT): A procedure similar to that used for **PPZ**-**DPO** was followed, but with 3-(4-bromophenyl)-4.5-diphenyl-1,2,4-triazole (1.88 g, 5 mmol) instead of 3-(4-bromophenyl)-5-phenyl-1,2,4-oxadiazole. After evaporation of the solvent, the crude product was subjected to column chromatography on silica gel (toluene: ethyl acetate = 2:1), giving the desired compound as a yellow powder with a yield of 64%. ^{1}H NMR (DMSO-d_6, 500 MHz): δ [ppm] 7.70–7.67 (m, 4H), 7.55–7.48 (m, 6H), 7.43–7.38 (m, 9H), 6.30–6.27 (m, 4H), 5.52–5.47 (m, 4H). ^{13}C NMR (DMSO-d_6, 125 MHz): δ [ppm] 154.4, 153.7, 141.0, 139.4, 136.1, 135.4, 134.8, 131.5, 130.8, 129.9, 129.7, 128.5, 128.3, 126.9, 121.2, 120.9, 112.4, 112.3. APCI-MS m/z: 554 [M+1]$^{+}$. Anal. calcd for $C_{38}H_{27}N_5$: C, 82.44; H, 4.92; N, 12.65. Found: C, 82.35; H, 4.92; N, 12.57.

4-[4-(5-Phenyl-5,10-dihydrophenazine)phenyl]-3,5-diphenyl-1,2,4-triazole (PPZ -4TPT): A procedure similar to that used for **PPZ**-**DPO** was followed but with 4-(4-bromophenyl)-3,5-diphenyl-1,2,4-triazole (1.88 g, 5 mmol) instead of 3-(4-bromophenyl)-5-phenyl-1,2,4-oxadiazole. After evaporation of the solvent, the crude product was subjected to column chromatography on silica gel (toluene: ethyl acetate

= 2:1), giving the desired compound as a yellow powder with a yield of 54%. ^{1}H NMR (DMSO-d_6, 500 MHz): δ [ppm] 7.72–7.68 (m, 4H), 7.55–7.52 (m, 3H), 7.50–7.40 (m, 12H), 6.37–6.30 (m, 4H), 5.53 (d, J = 7.5 Hz, 2H), 5.47 (d, J = 7.5 Hz, 2H). ^{13}C NMR (DMSO-d_6, 125 MHz): δ [ppm] 154.2, 140.7, 139.4, 136.0, 135.4, 134.6, 132.5, 131.9, 131.6, 130.7, 129.8, 128.6, 128.5, 128.4, 126.9, 121.3, 120.9, 112.3, 112.1. APCI-MS m/z: 555 [M+1]$^+$. Anal. calcd for $C_{38}H_{27}N_5$: C, 82.44; H, 4.92; N, 12.65. Found: C, 82.53; H, 4.83; N, 12.58.
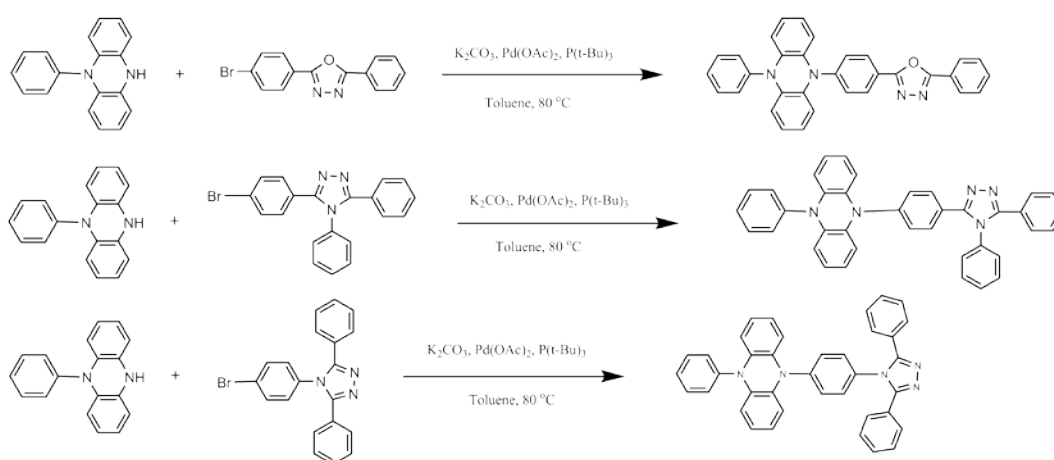
Figure 2-8. Synthesizing scheme of **PPZ-DPO, PPZ-3TPT** and **PPZ-4TPT.**

Photoluminescence measurements:

Solutions of the samples (0.1 mM) for luminescence studies were degassed with nitrogen for several minutes before use. Thin-film samples (~100 nm) for luminescence and photoelectron spectroscopy studies were deposited on quartz glass substrates by vacuum evaporation (pressure, <4 × 1024 Pa; rate, ~0.2 nm s^{-1}). UV–vis absorption spectra of the compounds in toluene were measured on a Perkin–Elmer Lambda 950-PKA UV–vis spectrophotometer in the range of 280–600 nm. Photoluminescence spectra were recorded on a Jasco FP-6500 spectrofluorometer equipped with a liquid nitrogen attachment at room temperature and 77 K. Absolute

PLQYs were obtained using a Quantaurus-QY measurement system (C11347-11, Hamamatsu Photonics) and all samples were excited at 380 nm. The PLQYs of the film samples were measured under nitrogen flow. The transient photoluminescence decay characteristics of solution samples were recorded using a Quantaurus-Tau fluorescence lifetime measurement system (C11367-03, Hamamatsu Photonics). The fast decay component was recorded in TCC900 mode in conjunction with LED excitation, while the slow decay component was recorded in M9003-01 mode with excitation by a 340 nm flash lamp. The emission decay of both the fast and slow components was well fitted by a single exponential. Two-dimensional transient decay (streak) images of the transient photoluminescence of the film samples were investigated under vacuum conditions using a streak camera (C4334, Hamamatsu Photonics) equipped with a Nd:YAG pulsed laser (λ=266 nm, pulse width $\approx$ 10 ns, repetition rate =10 Hz) as the excitation source. For TADF emitter-doped **mCP** films, the emission decay of the fast components was best fitted by a single exponential, while that of the slow component was best fitted with two exponentials. The average lifetime (τ_{av}) can be calculated using $\tau_{av}=\Sigma A_i\tau_i^2/\Sigma A_i\tau_i$, where A_i is the pre-exponential for lifetime τ_i. The HOMO energy levels of the compounds in the films were determined by atmospheric ultraviolet photoelectron spectroscopy using a photoelectron emission spectrometer (Riken Keiki AC-3).

Device Fabrication and Measurements:

After the precleaned **ITO**-coated glass substrates were treated with ozone for 15 min, the organic layers were deposited consecutively on the substrates in an inert chamber under a pressure of <4 $\times$ 10^{-4} Pa. Next, the cathode was fabricated by thermal evaporation of a LiF layer (1.0 nm), followed by an Al layer (100 nm). The deposition rates of the organic and Al layers were 0.1–0.2 nm s^{-1}, while that of the LiF layer was 0.01 nm s^{-1}. The intersection of the ITO and metal electrodes gave an active

device area of 4 mm^2. The current density J, voltage V and luminance L characteristics of the OLEDs were measured in ambient air with a semiconductor parameter analyser (E5273A, Agilent) and optical power meter (1930C, Newport). Electroluminescence spectra were recorded using a multichannel spectrometer (PMA12, Hamamatsu Photonics).

References

1. Tanaka, H.; Shizu, K.; Nakanotani, H.; Adachi, C., Twisted Intramolecular Charge Transfer State for Long-Wavelength Thermally Activated Delayed Fluorescence. *Chemistry of Materials* **2013**, *25*, 3766-3771.

2. Serevicius, T.; Nakagawa, T.; Kuo, M. C.; Cheng, S. H.; Wong, K. T.; Chang, C. H.; Kwong, R. C.; Xia, S.; Adachi, C., Enhanced electroluminescence based on thermally activated delayed fluorescence from a carbazole-triazine derivative. *Physical Chemistry Chemical Physics* **2013**, *15*, 15850-15855.

3. Nasu, K.; Nakagawa, T.; Nomura, H.; Lin, C. J.; Cheng, C. H.; Tseng, M. R.; Yasuda, T.; Adachi, C., A highly luminescent spiro-anthracenone-based organic light-emitting diode exhibiting thermally activated delayed fluorescence. *Chemical Communications* **2013**, *49*, 10385-10387.

4. Li, J.; Nakagawa, T.; Macdonald, J.; Zhang, Q.; Nomura, H.; Miyazaki, H.; Adachi, C., Highly efficient organic light-emitting diode based on a hidden thermally activated delayed fluorescence channel in a heptazine derivative. *Advanced Materials* **2013**, *25*, 3319-3323.

5. Zhang, Q.; Li, J.; Shizu, K.; Huang, S.; Hirata, S.; Miyazaki, H.; Adachi, C., Design of efficient thermally activated delayed fluorescence materials for pure blue organic light emitting diodes. *Journal of the American Chemical Society* **2012,** *134*, 14706-14709.

6. Uoyama, H.; Goushi, K.; Shizu, K.; Nomura, H.; Adachi, C., Highly efficient organic light-emitting diodes from delayed fluorescence. *Nature* **2012,** *492*, 234-238.

7. Nakagawa, T.; Ku, S. Y.; Wong, K. T.; Adachi, C., Electroluminescence based on thermally activated delayed fluorescence generated by a spirobifluorene donor-acceptor structure. *Chemical Communications* **2012,** *48*, 9580-9582.

8. Lee, S. Y.; Yasuda, T.; Nomura, H.; Adachi, C., High-efficiency organic light-emitting diodes utilizing thermally activated delayed fluorescence from triazine-based donor--acceptor hybrid molecules. *Applied Physics Letters* **2012,** *101*, 093306.

9. Lee, J.; Shizu, K.; Tanaka, H.; Nomura, H.; Yasuda, T.; Adachi, C., Oxadiazole- and triazole-based highly-efficient thermally activated delayed fluorescence emitters for organic light-emitting diodes. *Journal of Materials Chemistry C* **2013,** *1*, 4599-4604.

10. Becke, A. D., Density-Functional Thermochemistry .3. The Role of Exact Exchange. *Journal of Chemical Physics* **1993,** *98*, 5648-5652.

11. Wetmore, S. D.; Boyd, R. J.; Eriksson, L. A., Comparison of Experimental and Calculated Hyperfine Coupling Constants. Which Radicals Are Formed in Irradiated Guanine? *The Journal of Physical Chemistry B* **1998,** *102*, 9332-9343.

12. Baldo, M. A.; Adachi, C.; Forrest, S. R., Transient analysis of organic electrophosphorescence. II. Transient analysis of triplet-triplet annihilation. *Physical Review B* **2000,** *62*, 10967-10977.

13. Song, D.; Zhao, S.; Luo, Y.; Aziz, H., Causes of efficiency roll-off in phosphorescent organic light emitting devices: Triplet-triplet annihilation versus triplet-polaron quenching. *Applied Physics Letters* **2010,** *97*, 243304.

14. Reineke, S.; Walzer, K.; Leo, K., Triplet-exciton quenching in organic phosphorescent light-emitting diodes

with Ir-based emitters. *Physical Review B* **2007,** *75*, 125328.

15. Staroske, W.; Pfeiffer, M.; Leo, K.; Hoffmann, M., Single-step triplet-triplet annihilation: An intrinsic limit for the high brightness efficiency of phosphorescent organic light emitting diodes. *Physical Review Letters* **2007,** *98*, 197402.

16. Wang, Q.; Oswald, I. W. H.; Perez, M. R.; Jia, H. P.; Gnade, B. E.; Omary, M. A., Exciton and Polaron Quenching in Doping-Free Phosphorescent Organic Light-Emitting Diodes from a Pt(II)-Based Fast Phosphor. *Advanced Functional Materials* **2013,** *23*, 5420-5428.

17. Murawski, C.; Leo, K.; Gather, M. C., Efficiency Roll-Off in Organic Light-Emitting Diodes. *Advanced Materials* **2013,** *25*, 6801-6827.

18. Masui, K.; Nakanotani, H.; Adachi, C., Analysis of exciton annihilation in high-efficiency sky-blue organic light-emitting diodes with thermally activated delayed fluorescence. *Organic Electronics* **2013,** *14*, 2721-2726.

19. Huang, S.-T.; Liaw, D.-J.; Hsieh, L.-G.; Chang, C.-C.; Leung, M.-K.; Wang, K.-L.; Chen, W.-T.; Lee, K.-R.; Lai, J.-Y.; Chan, L.-H.; Chen, C.-T., Synthesis and electroluminescent properties of polyfluorene-based conjugated polymers containing bipolar groups. *Journal of Polymer Science Part A: Polymer Chemistry* **2009,** *47*, 6231-6245.

20. Terada, E.; Okamoto, T.; Kozaki, M.; Masaki, M. E.; Shiomi, D.; Sato, K.; Takui, T.; Okada, K., Exchange interaction of 5,5 '-(m- and p-phenylene)bis(10-phenyl-5,10-dihydrophenazine) dications and related analogues. *Journal of Organic Chemistry* **2005,** *70*, 10073-10081.

21. Xu, Q. L.; Li, H. Y.; Wang, C. C.; Zhang, S.; Li, T. Y.; Jing, Y. M.; Zheng, Y. X.; Huang, W.; Zuo, J. L.; You, X. Z., Synthesis, structure, photophysical and electrochemical properties of series of new fac-triscyclometallated iridium complexes with carbazole or oxadiazole moieties. *Inorganica Chimica Acta* **2012,** *391*, 50-57.

22. Kwon, S.; Wee, K. R.; Kim, A. L.; Kang, S. O., Bis(4-(4,5-diphenyl-4H-1,2,4-triazol-3-yl)phenyl) dimethylsilane as Electron-Transport Material for Deep Blue Phosphorescent OLEDs. *Journal of Physical Chemistry Letters* **2010,** *1*, 295-299.

23. Bedford, R. B.; Betham, M., N-H carbazole synthesis from 2-chloroanilines via consecutive amination and C-H activation. *Journal of Organic Chemistry* **2006,** *71*, 9403-9410.

Chapter 3

Monomeric and dimeric carbazolylcyanobenzenes as thermally activated delayed fluorescence emitters: Effect of substitution position on photoluminescent and electroluminescent properties

3.1 Introduction

From the discussion in Chapter 2, we concluded that both a small overlap between HOMO and LUMO and a higher ^{3}LE than ^{3}CT levels are crucial issues for realizing efficient TADF emitters. Based on this conclusion, we carefully designed a new series of D-A type TADF molecules using carbazole as a donor and cyano substituted benzene as an acceptor. Carbazole and cyano-benzene units have rather short π-conjugation length that is appropriate for the construction of blue TADF emitters. In this chapter, I will show four efficient blue and blue-green TADF emitters based on monomeric or dimeric carbazolylcyanobenzenes derivatives. In comparison with 3,5-dicyano substituted derivatives, 9,9'-bis(3,5-dicyano-phenyl)-3,3'-bicarbazolyl (**3-bis-5-CzIPN**) and 9-(3,5-dicyanolphenyl)-carbazolyl (**5-CzIPN**), the 2,6-dicyano substituted derivatives, 9,9'-bis(2,6-dicyano-phenyl)-3,3'-bicarbazolyl (**3-bis-2-CzIPN**) and 9-(2,6-dicyanolphenyl)-carbazolyl (**2-CzIPN**), provided larger dihedral angles, smaller ΔE_{ST} and shorter TADF transient lifetimes. An OLED based on **3-bis-2-CzIPN** gave an EQE of 10% with reduced efficiency roll-off characteristics. Besides the spatial distributions of HOMO and LUMO, the three excited-states model was also used to explain the difference of TADF lifetime and device efficiency roll-off characteristics in these carbazolyl cyanobenzenes.

3.2 Molecular structure and calculation results

The chemical structures of **5-CzIPN**, **2-CzIPN**, **3-bis-5-CzIPN** and **3-bis-2-CzIPN** are shown in Fig. 3-1. The synthesis of these monomeric and dimeric carbazolylcyanobenzenes derivatives was accomplished by the procedures described in the experimental section.
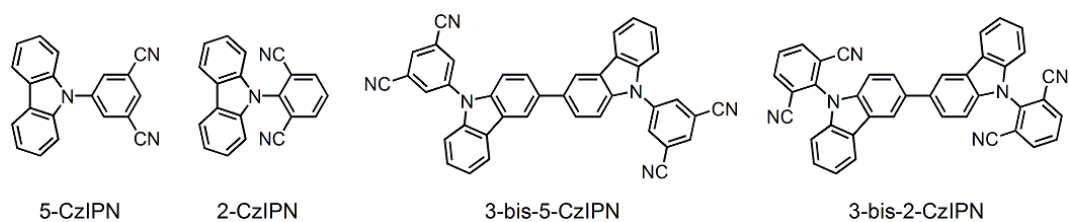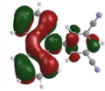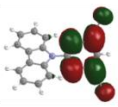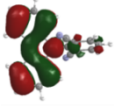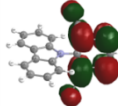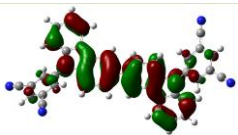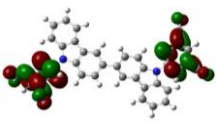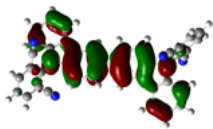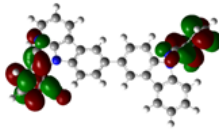
Figure 3-1. Chemical structures of **5-CzIPN, 2-CzIPN, 3-bis-5-CzIPN** and **3-bis-2-CzIPN**.

A small overlap between occupied and unoccupied molecular orbitals involved in the radiative transition is necessary to achieve a small ΔE_{ST}, although charge-transfer (CT) compounds may not provide CT characteristic of their T_1 states in some cases.[1, 2] In comparison with a typical TADF emitter of carbazolyl dicyanobenzene (**CDCB**) derivatives such as 2,4,5,6-tetrakis(carbazol-9-yl)-1,3- dicyanobenzene (**4CzIPN**),[3] the previously reported phenylcarbazole and triphenylamine based blue and red TADF emitters have relatively small dihedral angles between their donor and acceptor moieties, leading to a less efficient separation of their HOMO and LUMO.[4, 5] To better understand the influence of the twisting angle in D-A compounds on the nature of the electronic excited states, the ground-state geometries of **5-CzIPN**, **2-CzIPN**, **3-bis-5-CzIPN** and **3-bis-2-CzIPN** were optimized using density functional theory (DFT) at the B3LYP/6-31G* level.

As shown in Table 3-1, spatial distribution of the HOMO is mainly over the carbazole moieties, while that of the LUMO is completely localized over the dicyanobenzene moieties, indicating a CT characteristic of these compounds. The calculated results demonstrate that the substitution position influences on the twisting angle between the carbazole and dicyanobenzene planes. For the 2,6-dicyano substituted derivatives, **3-bis-2-CzIPN** and **2-CzIPN**, the twisting angles are around 69º, while those of 3,5-dicyano substituted derivatives, **3-bis-5-CzIPN** and **5-CzIPN**, are around 50º.[1, 2] Increasing the twisting angle between the donor and acceptor subunits minimizes the overlap of the HOMO and LUMO. As a result, time-dependent density functional theory (TD-DFT/B3LYP/6-31G*) calculation on

45

the basis of the ground state structures indicated relatively small ΔE_{ST} of 0.10 eV for **2-CzIPN** and 0.10 eV for **3-bis-2-CzIPN**, as compared to that of 0.20 eV for **5-CzIPN** and 0.20 eV for **3-bis-5-CzIPN**.

Table 3-1. Calculation results of **5-CzIPN**, **2-CzIPN**, **3-bis-5-CzIPN** and **3-bis-2-CzIPN**.

	HOMO	LUMO	S_1 (eV)	T_1 (eV)	ΔE_{ST} (eV)
5-CzIPN			2.97	2.78	0.19
2-CzIPN			2.83	2.76	0.07
3-bis-5-CzIPN			2.79	2.66	0.13
3-bis-2-CzIPN			2.60	2.57	0.03

3.3 Photophysical characteristics

The absorption and fluorescence spectra at 300 K and the phosphorescence spectra at 77 K of **5-CzIPN**, **2-CzIPN**, **3-bis-5-CzIPN** and **3-bis-2-CzIPN** in toluene at a concentration of 10^{-5} mol/L are shown in Fig. 3-2. The large stokes shift and broad structureless fluorescence bands with the full width at half maximum (FWHM) over 70 nm clearly imply CT character of their S_1 to S_0 transitions. The emission peaks of **3-bis-5-CzIPN** and **3-bis-2-CzIPN** locate at 470 nm and 488 nm which are red-shifted by 35 nm and 45 nm with respect to their corresponding monomers, **2-CzIPN** and **5-CzIPN**, respectively. The redshift of the emission peaks can be explained by the extension of π-conjugation through the carbazole-carbazole bonding.

It makes not only the HOMO energy levels shallower (see Table 3-1) but also the optical energy-gap (E_g) narrower.
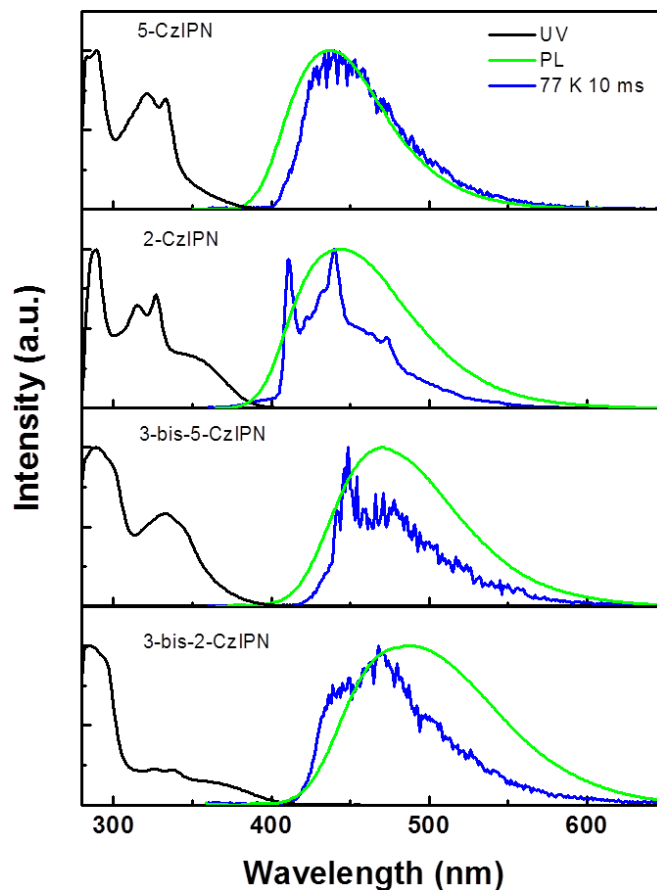

Figure 3-2. Absorption and emission spectra of 5-CzIPN, 2-CzIPN, 3-bis-5-CzIPN and 3-bis-2-CzIPN in toluene at 300 RT and their phosphorescence spectrum at 77 K with 10 ms delay.

Table 3-2. Excited-state energy and molecular orbital data for carbazolylcyanobenzenes in oxygen-free toluene at RT (unit of all the data is eV).

Parameter	5-CzIPN	2-CzIPN	3-bis-5-CzIPN	3-bis-2-CzIPN
$E_{VE}(S_1)^a$	2.85	2.80	2.64	2.54
$E_{0-0}(S_1)$	3.18	3.16	3.00	2.83
$E_{0-0}(T_1)$	3.00	3.03	2.84	2.77
ΔE_{ST}	0.18	0.13	0.16	0.06
$E_g{}^b$	3.26	3.22	3.04	3.05
HOMO^c	6.28	6.22	6.08	6.05
LUMO^d	3.02	3.00	3.04	3.00

$^a E_{VE}(S_1)$ is the vertical emission energy estimated from the peak of the emission band. $^b E_g$ is the

optical band-gap determined from the absorption edge. [c]HOMO energy level was recorded in a neat film by AC-3. [d]LUMO energy level was obtained from the HOMO value minus E_g.

We can derive the ΔE_{ST} from the room temperature fluorescence spectra and the low temperature phosphorescence spectra by the same method described in Chapter 2. As noted above, the S_1 states of all these four compounds in toluene are CT states whose zero-zero energies (E_{0-0}) can be estimated from the onset of their emission bands (Table 3-2). On the other hand, from the characteristic phosphorescence spectrum showing clear vibration mode, we conclude that the T_1 state of **2-CzIPN** is a LE state, whose E_{0-0} is determined from the highest energy peak of its emission band. On the basis of the E_{0-0} values of S_1 and T_1 states, the ΔE_{ST} of **2-CzIPN** in toluene at RT was calculated to be 0.13 eV (Table 3-2). In contrast, the T_1 states of **5-CzIPN**, **3-bis-5-CzIPN** and **3-bis-2-CzIPN** are based on CT and LE mixed states, in which the CT characteristic is dominant.[1, 6] Their ΔE_{ST} in toluene at RT are calculated to be 0.18, 0.16 and 0.06 eV, respectively (Table 3-2). The difference in ΔE_{ST} between the 3,5-dicyano substituted and the 2,6-dicyano substituted derivatives is in accordance with the TD-DFT predictions (Table 3-1) and can explain their different TADF rate constants as will be discussed below.
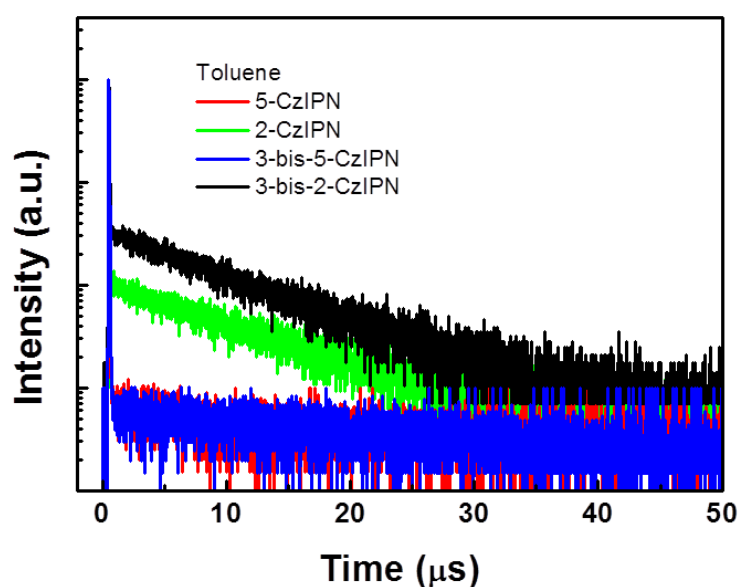
Figure 3-3. Transient decay spectra of **5-CzIPN**, **2-CzIPN**, **3-bis-5-CzIPN** and **3-bis-2-CzIPN** in degassed toluene at RT.

Table 3-3. Photophysical data for carbazolylcyanobenzenes in oxygen-free toluene at RT.

Parameter	5-CzIPN	2-CzIPN	3-bis-5-CzIPN	3-bis-2-CzIPN
Φ_F	0.10	0.07	0.26	0.24
Φ_{TADF}	0.02	0.15	0.32	0.48
τ_F (ns)	24	14	24	28
τ_{TADF} (μs)	28	9.4	145	9.2
k_F ($\times 10^7$ s^{-1})	0.42	0.50	1.08	0.86
k_{TADF} ($\times 10^4$ s^{-1})	0.07	1.6	0.17	5.2
ΔE_{ST} (eV)	0.18	0.13	0.16	0.06

The transient PL characteristics of **5-CzIPN**, **2-CzIPN**, **3-bis-5-CzIPN** and **3-bis-2-CzIPN** in oxygen-free toluene at RT are shown in Fig. 3-3. All compounds show two-component decays. A fast decay with a lifetime (τ) at nanosecond order can be assigned to normal fluorescence, while a slow component with a much longer lifetime of micro second corresponds to the TADF decay, which cannot be observed in air-saturated solutions. Their individual excited-state lifetimes of fluorescence and TADF are summarized in Table 3-3. In oxygen-free toluene at RT,[7-9] the photoluminescence quantum yields (PLQY: Φ) of **5-CzIPN**, **2-CzIPN**, **3-bis-5-CzIPN** and **3-bis-2-CzIPN** are estimated to be 0.12, 0.22, 0.50 and 0.72, respectively. By comparing the integral of each emission component in the transient decay spectra, the individual PLQY values of fluorescence (Φ_F) and TADF (Φ_{TADF}) can be distinguished from the total PLQY (Table 3-3). Then, the rate constants of fluorescence (k_F) and TADF (k_{TADF}) can be calculated using equations (1) and (2).

$$k_F = \Phi_F/\tau_F \quad (1)$$

$$k_{TADF} = \Phi_{TADF}/\tau_{TADF} \quad (2)$$

As listed in Table 3-3, the rate constants of the fluorescence were almost independent of the substitution position, while the rate constants of the TADF were

considerably different. As revealed by D. R. McMillin et al., the relationships among the observed rate of delayed emission (k_{obs}), k_F and ΔE_{ST} can be expressed as a Boltzmann average.

$$k_{obs} = (k_F K + k_P)/(1+K) \qquad (3)$$

$$K = 1/3 \exp(-\Delta E_{ST}/RT) \qquad (4)$$

Here, k_P, R, T, and 1/3 denote the rate constant of phosphorescence, ideal gas constant, absolute temperature, and the ratio of the degeneracies of S_1 to T_1 states, respectively. For aromatic compounds, k_F and k_P are generally $10^6 \sim 10^9$ s^{-1} and $10^{-2} \sim 1$ s^{-1}, respectively. Therefore, $k_{P,CT} \ll k_F K$ is expected at RT when ΔE_{ST} is smaller than 0.3 eV ($K > 3.0 \times 10^{-6}$). Moreover, if ΔE_{ST} is larger than 0.05 eV (*i.e.*, $K < 0.05$ at 300 K), equation (4) can be simplified to:

$$k_{obs} = k_{TADF} = k_F K \qquad (5)$$

Accordingly, k_{TADF} is approximately proportional to k_F while it is inversely proportional to $\exp(\Delta E_{ST})$ at RT. To test the reliability of equation (5), I calculated the ΔE_{ST} of all these compounds from it using the k_F and k_{TADF} data in Table 3-3, and found these calculated values are consistent with the experimental results (Table 3-2) determined from the fluorescence and phosphorescence spectra.

For OLED application, it is crucial to find a suitable host material that maximizes harvesting of triplet excitons for EL. The PLQYs of **3-bis-5-CzIPN** and **3-bis-2-CzIPN** in 10 wt%-doped 1,3-bis(carbazol-9-yl)benzene (**mCP**, T_1 = 2.9 eV) films were estimated to be 0.29 and 0.48, respectively. However, by using bis(2-(diphenylphosphino)phenyl)ether oxide (**DPEPO**, T_1 = 3.3 eV) as a host, the PLQYs of **3-bis-5-CzIPN** and **3-bis-2-CzIPN** were dramatically improved to be 0.58 and 0.72, respectively. Therefore, a high triplet energy host of **DPEPO** was used for both PL and EL measurements in this study. The PLQYs of **5-CzIPN** and **2-CzIPN** were estimated to be 0.41 and 0.22, respectively, in the doped **DPEPO** films.
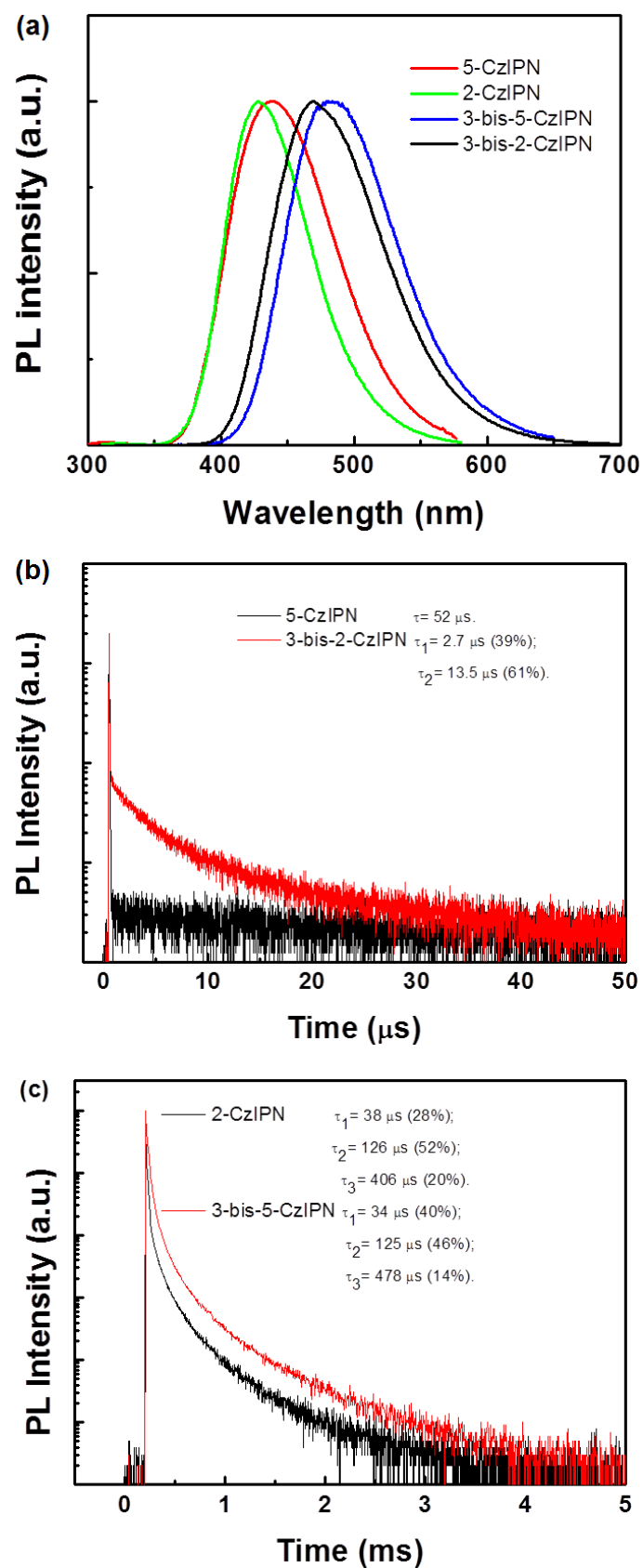
Figure 3-4. PL spectra (a) and their transient decay spectra (b,c) of **5-CzIPN**, **2-CzIPN**, **3-bis-5-CzIPN** and **3-bis-2-CzIPN** doped into a **DPEPO** host with a concentration of 10 wt%.

Fig. 3-4 shows the PL spectra (a) and transient decay curves (b and c) of these emitters in 10 wt%-doped films using **DPEPO** as a host. The emission spectra of these compounds in a **DPEPO** film are almost identical to those in the toluene solution. The slow components with the transient lifetime on the order of microseconds can be ascribed to TADF. Their emission decays are fitted with single to three exponentials as shown in Fig. 3-4. The average lifetime (τ_{av}) of multi-exponentials is calculated using $\tau_{av} = \Sigma A_i \tau_i^2 / \Sigma A_i \tau_i$, where A_i is the pre-exponential for lifetime τ_i. Accordingly, the $\tau_{av,TADF}$ of **5-CzIPN**, **2-CzIPN**, **3-bis-5-CzIPN** and **3-bis-2-CzIPN** in doped films are calculated to be 52, 155, 137 and 9.3 μs, respectively. In the doped **DPEPO** films, the TADF lifetimes of **5-CzIPN**, **3-bis-5-CzIPN** and **3-bis-2-CzIPN** are comparable with the corresponding values in toluene (Table 3-3). However, for **2-CzIPN**, its TADF lifetime in the doped film is clearly longer than that in toluene, probably because of the change of its ΔE_{ST} in the solid matrix.
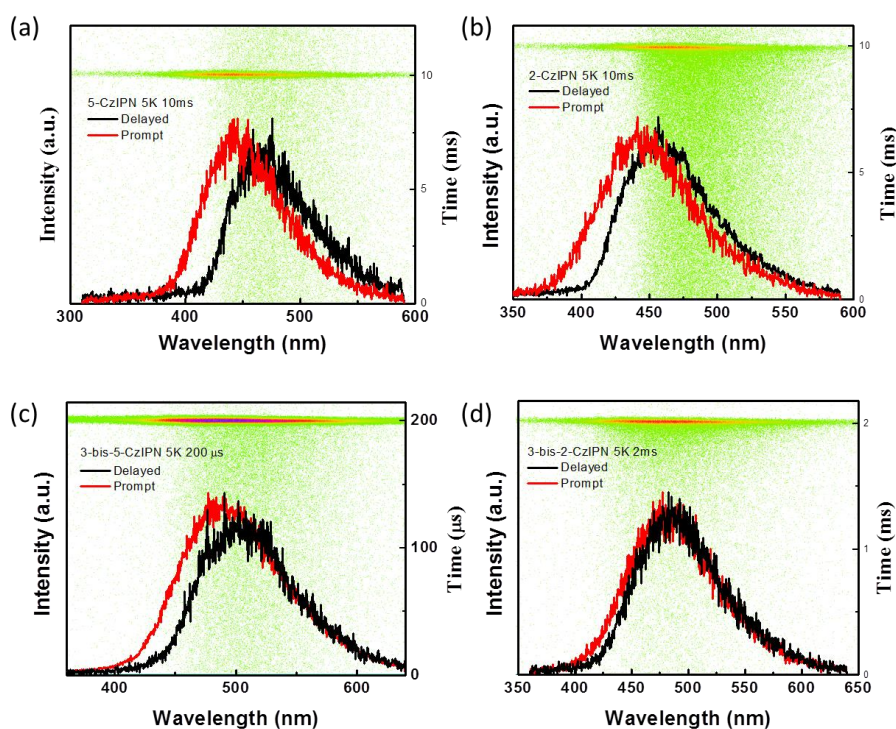

Figure 3-5. Streak images (transient PL) of **5-CzIPN** (a), **2-CzIPN** (b), **3-bis-5-CzIPN** (c) and **3-bis-2-CzIPN** (d) doped into a **DPEPO** host with a concentration of 10 wt% at 5 K.

Fig. 3-5 shows the streak images of **5-CzIPN**, **2-CzIPN**, **3-bis-5-CzIPN** and **3-bis-2-CzIPN** doped into a DPEPO host measured at 5 K. The ΔE_{ST} determined from the difference between the fluorescence and phosphorescence onset are 0.18, 0.18, 0.14 and 0.06 eV for **5-CzIPN**, **2-CzIPN**, **3-bis-5-CzIPN** and **3-bis-2-CzIPN**, respectively, in the doped **DPEPO** films. In comparison with the ΔE_{ST} values determined in toluene (Table 3-2), that of **2-CzIPN** in the doped film enlarges significantly, which explains the increase of the TADF lifetime in the film. It is found that the emission band of **2-CzIPN** in the doped film (Fig. 3-4a) is slightly blue shifted compared with that observed in toluene (Fig. 3-2) because the rigid matrix inhibits the considerable conformational relaxation in the charge transfer excited state and reduces the Stokes shift, leading to an increase of the S_1 energy (0.05 eV). In contrast, the E_{0-0} of the T_1 state of **2-CzIPN** is insensitive to the environment because of its ^{3}LE nature as mentioned above. As a result, the 2,6-dicyano substituted derivative **2-CzIPN** has a relatively large ΔE_{ST} in the doped film, in spite of the sufficiently separated orbitals involved in the emissive transition and a small ^{1}CT–^{3}CT splitting.

3.4 OLED performance

As shown in Fig. 3-6, using 10 wt% carbazolylcyanobenzenes doped **DPEPO** films as emitting layers (EMLs), four multilayer OLEDs were fabricated with a configuration of **ITO/α-NPD** (30 nm)/**mCP** (10 nm)/emitter in **DPEPO** (10 wt%, 15 nm)/**TPBI** (60 nm)/LiF (0.8 nm)/Al (100 nm), where **α-NPD**, and **TPBI** represent N,N′-diphenyl-N,N′-bis(1-naphthyl)-1,10-biphenyl-4,4′-diamine, and 1,3,5-tris(N-phenylbenzimidazol-2-yl)benzene. Here, a thin layer of **mCP** was inserted between a hole injection layer (**α-NPD**) and an emitting layer to reduce the energy barriers and help hole injection from the anode. A thin layer of **DPEPO** between the ETL of **TPBI** and the EML was employed to provide efficient exciton blocking.
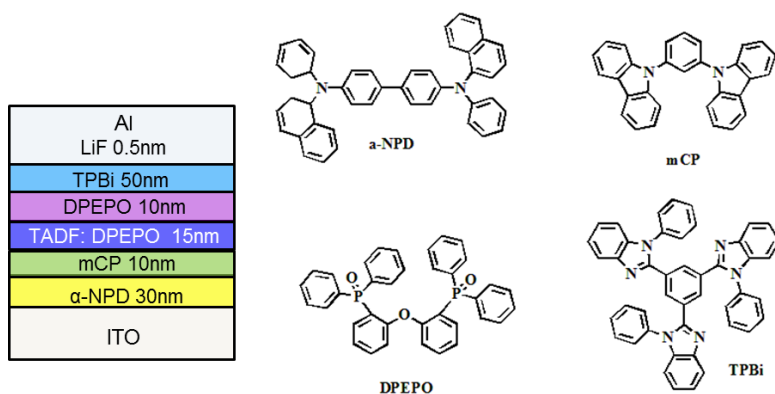
Figure 3-6. Device configuration and molecular structures utilized in this experiment.

Fig. 3-7 demonstrates EQE-current density characteristics, luminance-voltage characteristics, current density-voltage characteristics, and EL spectra of the devices based on **5-CzIPN**, **2-CzIPN**, **3-bis-5-CzIPN** and **3-bis-2-CzIPN** as an emitter. The EL spectra of these OLEDs coincided with their PL spectra in the **DPEPO** films. Among these devices, **3-bis-5-CzIPN** and **3-bis-2-CzIPN** based OLEDs show the highest external quantum efficiency (EQE) because of their relatively high PLQY of 0.58 and 0.72 in the doped **DPEPO** films. At a low current density of 0.05 mA/cm^2, the EQEs of the **3-bis-5-CzIPN** and **3-bis-2-CzIPN** based devices were as high as 9.2% and 9.6%, respectively, which are significantly higher than the theoretical limitation (5%) for fluorescent OLEDs. For TADF based OLEDs, the theoretical maximum of EQE can be estimated using the formula as follows,[6]

$$EQE = \eta_{\text{int}} \times \eta_{\text{out}} \qquad (6)$$

$$\eta_{\text{int}} = \Phi_{\text{F}} \times \chi_{\text{S}} + \Phi_{\text{TADF}} \times \chi_{\text{S}} + \Phi_{\text{TADF}} \times \chi_{\text{T}} \qquad (7)$$

where η_{int} is the theoretical maximal internal quantum efficiency, η_{out} is the light out-coupling efficiency (0.2–0.3), χ_{S} and χ_{T} are the branching ratios of singlet (0.25) and triplet (0.75) exciton formations, respectively. On the basis of the $\Phi_{\text{F}}/\Phi_{\text{TADF}}$ values of 0.26/0.32 for **3-bis-5-CzIPN** and 0.24/0.48 for **3-bis-2-CzIPN** obtained from the transient spectra of the doped films (Fig. 3-4), the theoretical maximal EQE of **3-bis-5-CzIPN** and **3-bis-2-CzIPN** based OLEDs are estimated to be 8-12% and

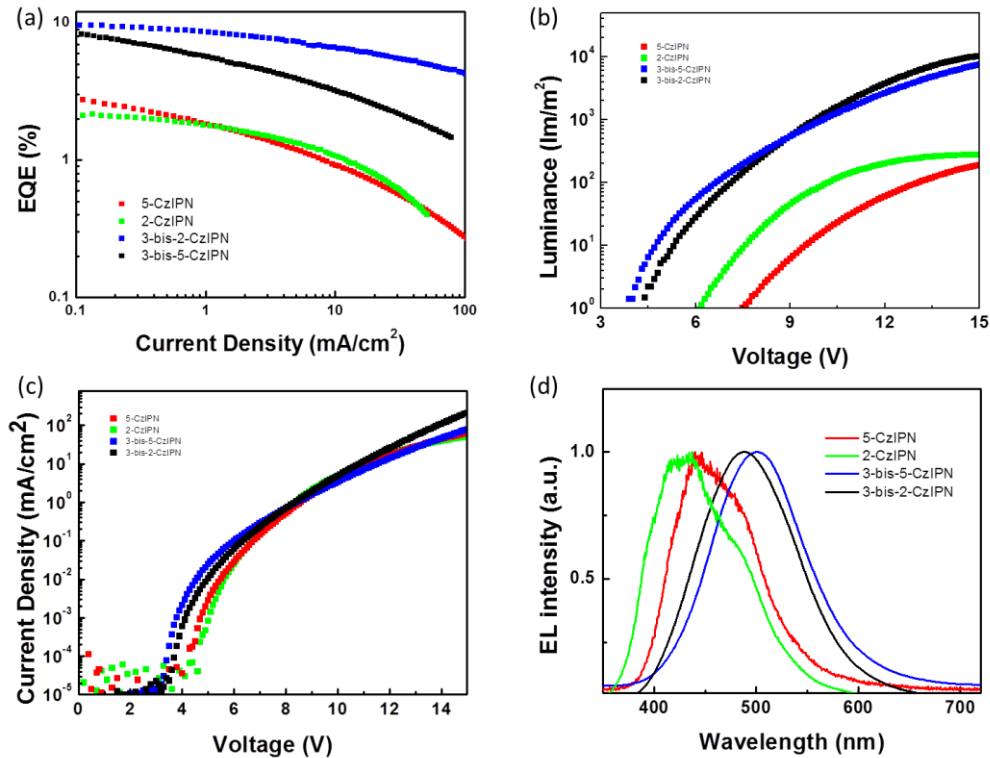10-15%, respectively, which is in good consistent with the experimental values.

Figure 3-7. EQE versus current density (a), luminance versus voltage (b), current density versus voltage (c), and EL spectra (d) of **5-CzIPN**, **2-CzIPN**, **3-bis-5-CzIPN** and **3-bis-2-CzIPN** based OLEDs.

Although a **3-bis-5-CzIPN** based OLED exhibited a high EQE at low current density, its EQE decreased dramatically with an increase in current density and was only 1.4% at 100 mA/cm^2. The rapid efficiency roll-off in a **3-bis-5-CzIPN** based OLED can be ascribed to the low TADF decay rate of the dopant which leads to critical triplet-triplet, triplet-polaron and singlet–triplet annihilations at high current density as discussed in Chapter 2. Because **3-bis-2-CzIPN** has a shorter TADF lifetime of a few microseconds, its device exhibited a reduced efficiency roll-off and maintained an EQE of 4.3% at 100 mA/cm^2. Since **5-CzIPN** and **2-CzIPN** also show low TADF decay rates in doped **DPEPO** films, the EQE roll-off of their devices at high current density were also significant.

3.5 Conclusion

In summary, I synthesized four new monomeric and dimeric carbazolylcyanobenzenes derivatives and observed the TADF phenomenon from all derivatives. By changing the substitution position of the cyano groups on the phenyl rings, the twisting angle between the donor and acceptor moieties could be adjusted. Ortho-substitution was found to lead to a larger twisting angle and a more efficient separation of the HOMO and LUMO. For the two dimeric carbazolylcyanobenzenes whose ^{3}LE states are higher than their ^{3}CT state, 2,6-dicyano substituted derivative (**3-bis-2-CzIPN**) resulted in a smaller ΔE_{ST}, a faster TADF decay rate, and reduced EL efficiency roll-off characteristics at high current density as compared with that of the analogous of the 3,5-dicyano substituted derivative, **3-bis-5-CzIPN**.

3.6 Experimental section

Synthesis

9-(3,5-dicyanolphenyl)-carbazolyl (5-CzIPN): A mixture of carbazole (3 g, 20.55 mmol), 5-chloroisophthalnitrile (4.13 g, 24.66 mmol) and K_2CO_3 (5.68 g, 41.1 mmol) suspended in 82 mL dry DMF was stirred and heated at 70 ℃ overnight. The cooled mixture was partitioned between chloroform and water. The organic layer was separated, and the aqueous layer was extracted with chloroform. The combined organic layers were dried over $MgSO_4$, and concentrated in vacuum. Purification of the residue by column chromatography (silica, chloroform/ethyl acetate = 1:1) afforded 3.20 g of 5CzIPN, with a yield of 49.7%. ^{1}H NMR (500 MHz, $CDCl_3$, TMS) $\delta =$ 7.369-7.402 (m, J=16.5 Hz, 4H), 7.467-7.500 (m, J=16.5 Hz, 2H), 7.992 (s, 1H), 8.147-8.166 (m, J=9.5 Hz, 4H). TOF-Mass [M+] calcd.: 293.32; found, 293.10.

9-(2,6-dicyanolphenyl)-carbazolyl (2-CzIPN): The ortho lithiation of 1,3-dicyanobenzene (5 g, 39.0 mmol) using lithium diisopropylaminde (LDA, 5 g) was completed in 30 mins at -96 ℃ in dry THF (450 ml). In sequence, the product was added CCl_3CCl_3 (14.75 g, 62.3 mmol) as electrophiles to get 2-chloroisophthalnitrile before warm up to room temperature. The cooled mixture was partitioned between dichloromethane and water. The organic layer was separated, and the aqueous layer was extracted with dichloromethane. The combined organic layers were dried over $MgSO_4$, and concentrated in vacuum. Purification of the residue by column chromatography (silica, chloroform/hexane = 3:1) afforded 5.36 g of 2CzIPN, with a yield of 42.3%.[10] ^{1}H NMR (500 MHz, $CDCl_3$, TMS) $\delta =$ 7.069-7.085 (d, J=8 Hz, 2H), 7.361-7.392 (m, J = 15.5 Hz, 2H), 7.440-7.473 (m, J = 21 Hz, 1H), 8.134-8.169 (m, J= 12.5 Hz, 4H). TOF-Mass [M+] calcd.: 293.32; found, 293.15.

9,9'-bis(3,5-dicyano-phenyl)-3,3'-bicarbazolyl (3-bis-5-CzIPN): A mixture of 3, 3'-dicarbazyl[11] (3 g, 9 mmol), 5-chloroisophthalnitrile (2.93 g, 18 mmol) and K_2CO_3 (4.98 g, 36 mmol) suspended in 78 mL dry DMF was stirred and heated at 70 ℃

overnight. The cooled mixture was partitioned between chloroform and water. The organic layer was separated, and the aqueous layer was extracted with chloroform. The combined organic layers were dried over MgSO$_4$, and concentrated in vacuum. Purification of the residue by column chromatography (silica, chloroform/ethyl acetate = 10:1) afforded 2.30 g of 3-bis-5-CzIPN, with a yield of 53.1%. ^{1}H NMR (500 MHz, CDCl$_3$, TMS) δ = 7.416-7.467 (m, 4H), 7.506-7.544 (m, 4H), 7.282 (dd, J=10.5 Hz, 2H), 8.021 (s, 2H), 8.217 (s, 4H) 8.256 (d, J=8 Hz, 2H), 8.450 (s, 2H). ^{13}C NMR (125 MHz, DMSO, TMS) δ = 140.01, 138.85, 138.68, 135.02, 134.82, 133.97, 126.77, 125.74, 123.98, 123.41, 121.11, 120.86, 118.62, 116.68, 114.82, 110.30, 109.96. TOF-Mass [M+] calcd.: 586.64; found, 584.04.

9,9'-bis(2,6-dicyano-phenyl)-3,3'-bicarbazolyl (3-bis-2-CzIPN): A mixture of 3, 3'-dicarbazyl (3 mmol, 1 g), 2-chloroisophthalonitrile (6 mmol, 1.8 g) and K$_2$CO$_3$ (1.66 g, 12 mmol) was stirred in 24 mL dry DMF and heated at 150 ℃ overnight. The cooled mixture was washed with CHCl$_3$ and MeOH. The obtained product was concentrated in vacuum. Purification of the residue by column chromatography (silica, acetone/ethyl acetate/hexane = 1:5:5) afforded 1.20 g of 3-bis-2-CzIPN, with a yield of 68.5%. ^{1}H NMR (500 MHz, CDCl$_3$, TMS) δ =7.115 (d, J=4.5 Hz, 2H), 7.195 (d, J=8.5 Hz, 2H), 7.416 (t, J=7.5 Hz, 2H), 7.491 (t, J=7.5 Hz, 2H), 7.783-7.831 (m, 4H), 8.183 (d, J=4 Hz, 4H), 8.255 (d, J=7.5 Hz, 2H), 8.455 (s, 2H). ^{13}C NMR (125 MHz, CDCl3, TMS) δ =143.23, 140.62, 139.43, 138.36, 135.90, 129.49, 126.73, 126.58, 124.99, 124.56, 121.87, 121.12, 119.90, 115.75, 114.19, 109.69, 109.58. TOF-Mass [M+] calcd.: 586.64; found, 586.47.
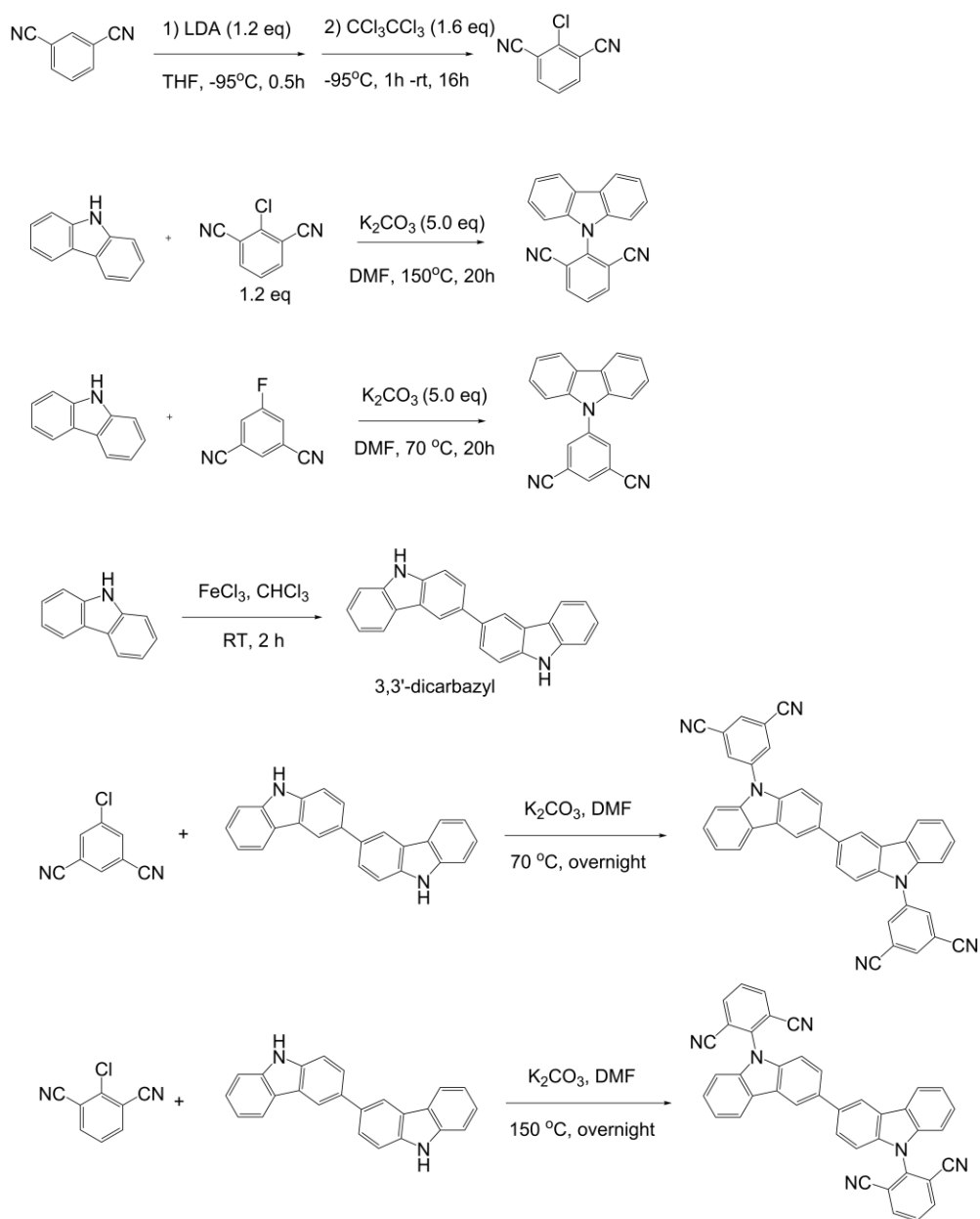
Figure 3-8. Synthesis of **5-CzIPN**, **2-CzIPN**, **3-bis-5-CzIPN** and **3-bis-2-CzIPN**.

References

1. Huang, S.; Zhang, Q.; Shiota, Y.; Nakagawa, T.; Kuwabara, K.; Yoshizawa, K.; Adachi, C., Computational Prediction for Singlet- and Triplet-Transition Energies of Charge-Transfer Compounds. *Journal of Chemical Theory and Computation* **2013,** *9*, 3872-3877.

2. Lu, T.; Chen, F., Multiwfn: a multifunctional wavefunction analyzer. *Journal of Computational Chemistry* **2012,** *33*, 580-592.

3. Uoyama, H.; Goushi, K.; Shizu, K.; Nomura, H.; Adachi, C., Highly efficient organic light-emitting diodes from delayed fluorescence. *Nature* **2012,** *492*, 234-238.

4. Li, J.; Nakagawa, T.; Macdonald, J.; Zhang, Q.; Nomura, H.; Miyazaki, H.; Adachi, C., Highly efficient organic light-emitting diode based on a hidden thermally activated delayed fluorescence channel in a heptazine derivative. *Advanced Materials* **2013,** *25*, 3319-3323.

5. Zhang, Q.; Li, J.; Shizu, K.; Huang, S.; Hirata, S.; Miyazaki, H.; Adachi, C., Design of efficient thermally activated delayed fluorescence materials for pure blue organic light emitting diodes. *Journal of the American Chemical Society* **2012,** *134*, 14706-14709.

6. Zhang, Q.; Li, B.; Huang, S.; Nomura, H.; Tanaka, H.; Adachi, C., Efficient blue organic light-emitting diodes employing thermally activated delayed fluorescence. *Nature Photonics* **2014,** *8*, 326-332.

7. Ottolenghi, M.; Goldschmidt, C. R.; Potashnik, R., Intersystem crossing in the charge-transfer quenching of molecular fluorescence. *The Journal of Physical Chemistry* **1971,** *75*, 1025-1031.

8. Abdel-Shafi, A. A.; Worrall, D. R., Mechanism of the excited singlet and triplet states quenching by molecular oxygen in acetonitrile. *Journal of Photochemistry and Photobiology a-Chemistry* **2005,** *172*, 170-179.

9. Cabrerizo, F. M.; Arnbjerg, J.; Denofrio, M. P.; Erra-Balsells, R.; Ogilby, P. R., Fluorescence Quenching by Oxygen: "Debunking" a Classic Rule. *Chem. Phys. Chem.* **2010,** *11*, 796-798.

10. Krizan, T. D.; Martin, J. C., Directed ortho lithiation of isophthalonitrile. New methodology for the synthesis of 1,2,3-trisubstituted benzenes. *The Journal of Organic Chemistry* **1982,** *47*, 2681-2682.

11. Yan, G.; Antisar, H.; Jinyan, W.; Ke, C.; Allan, S. H., Synthesis of Homo- and Copoly(arylene bicarbazole)s via Nucleophilic Substitution Polycondensation Reactions of NH Groups with Activated Dihalides. *Macromolecules* **2007,** *40*, 4744-4746.

Chapter 4

High efficiency blue thermally activated delayed fluorescence emitter with rapid delayed fluorescence rate and reduced electroluminescence efficiency roll-off

4.1 Introduction

The three primary colors, red, green and blue, are necessary to achieve full color OLED display. After the report of highly efficient OLEDs in the late 80', blue, green and red emitting materials of different categories have been abundantly developed by many researchers.[1-6] Now, OLEDs having high luminance, power conversion efficiency and stability of green and red EL have achieved the requirements for commercialization by employing phosphorescent dopants.[1] However, efficient and stable deep-blue OLEDs are still problematic because of the following reasons. (1) The blue phosphorescent emitters are still largely limited to sky-blue emissions such as **Firpic** and its analogues.[1-9] Pure blue phosphorescent emitters are always inefficient and unstable because the unstable and nonluminescent excited d–d states in d^6 and d^8 transition metal complexes become more thermally populated when the energies of their emissive excited states is enhanced.[3, 10] (2) Blue fluorescent OLEDs are relatively stable compared with blue phosphorescent OLEDs. However, deep blue fluorescent OLEDs generally have an EQE of less than 5% because only the singlet excitons (25%) can emit light as far as we use conventional fluorescent emitters.[11] (3) An alternative approach for efficient blue OLEDs is to increase singlet exciton generation in fluorescent OLEDs through triplet-triplet annihilation (TTA) and charge-transfer induced spin transition.[12] In 2012, Y. G. Ma group demonstrated a maximum EQE of >5.0% in a deep blue OLED using a charge-transfer triphenylamine/imidazol derivative as an emitter.[13] The intercrossed excited-state character of the emitter is thought to be beneficial for the improved EQE. In 2013, J. Kido et al. reported a deep blue OLED based on an anthracene derivative. The maximum EQE as high as 12% was ascribed to the increased singlet excitons resulting from a TTA process.[14] However, the singlet generation fraction in both kinds of OLEDs cannot be higher than 63% (0.25+0.75×0.5) according to the theoretical analysis,[15] and the reliability of these blue OLEDs has not been reported.

In 2009, our group proposed the TADF process as an alternative scheme of traditional noble-metal-based organometallic phosphors.[16-21] In 2012, Q. Zhang et al. proposed a design principle for blue TADF emitters. Blue TADF only occurs in a donor-acceptor bipolar system where the donor and acceptor centered $^3\pi$-π^* state is close to or higher than the ^{3}CT state.[18] Basing on this concept, a series of sulfone derivatives were applied to OLEDs and demonstrated deep blue EL with an EQE of 10% at low current density. Since the short lifetime of blue PHOLEDs has not been overcome while a wide variety of molecular backbones were considered, it is most crucial to improve the lifetime by developing TADF based blue OLEDs. In this chapter, I demonstrate an efficient blue TADF based OLED that is as efficient as the best blue PHOLEDs. The structure–property relationships in blue TADF emitters are studied in detail.

4.2 Molecular structures and calculation results

As discussed in Chapters 2 and 3, a small ΔE_{ST} is necessary for efficient reverse intersystem crossing from T_1 to S_1 in TADF emitters. To achieve a small ΔE_{ST}, the exchange integral between the wave functions involved in the lowest-energy transition should be small. Although π-π^* charge-transfer (CT) transitions meet with this requirement, a locally excited $^3\pi$-π^* state (^{3}LE) is the lowest triplet state in most aromatic CT compounds.[22, 23] Therefore, another design principle for efficient TADF materials is that any ^{3}LE state should be close or higher than the ^{3}CT state.[18] I focused on the combination of the above two principles and obtained a blue TADF compound with high PLQY and short TADF lifetime. The molecules investigated in this work are shown in Fig. 4-1.
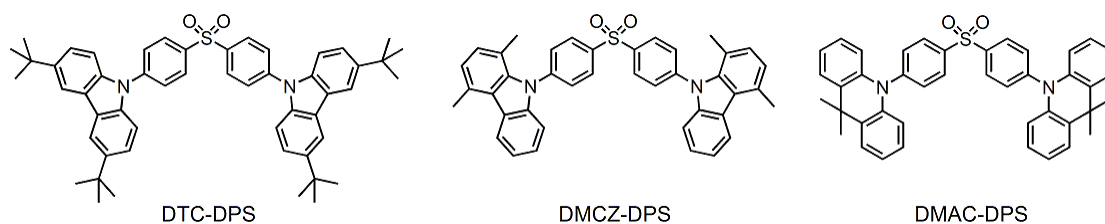
Figure 4-1. Molecular structures of **DTC-DPS**, **DMCZ-DPS** and **DMAC-DPS**.

According to the Q. Zhang's report, the EQE roll-off of bis[4-(3,6-di-tert-butylcarbazole)phenyl]sulfone (**DTC-DPS**)-based OLED is significant at high current density.[18] It was caused by the relatively large ΔE_{ST} and the long excited-state lifetime of **DTC-DPS**. For **DTC-DPS**, a $^3\pi$-π^* state localized at the carbazole unit was found to be the T_1 state of the whole molecule. The energy difference between ^{1}CT and ^{3}CT states is also relatively large in **DTC-DPS** because of the insufficient separation of its HOMO and LUMO.[9] Obviously, increasing the dihedral angle between donor and acceptor planes can reduce the exchange energy between the singlet and triplet CT states as demonstrated in Chapter 2. On the other hand, adjusting the relative energy levels of ^{3}CT and ^{3}LE states can further decrease the ΔE_{ST} value as demonstrated in Chapter 3. These molecular design concepts are shown in Fig. 4-2.
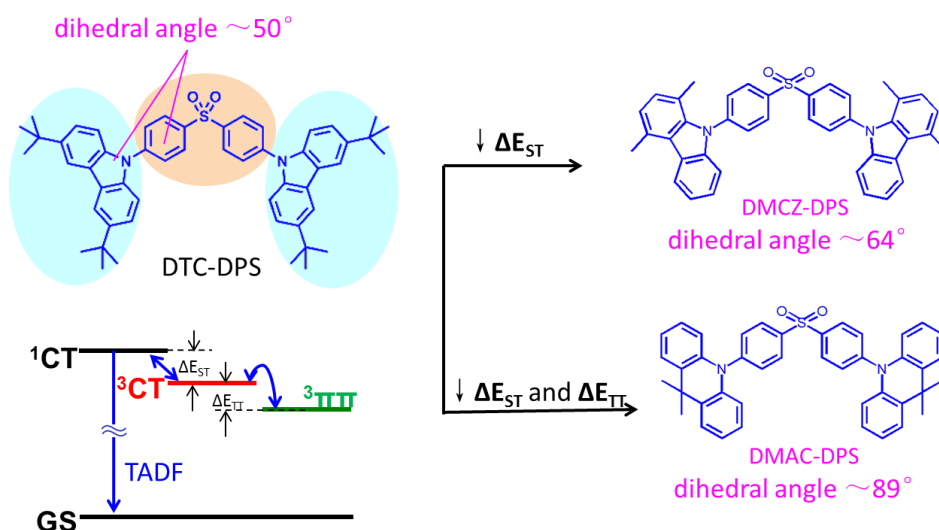

Figure 4-2. Energy diagrams and design concepts of **DMCZ-DPS** and **DMAC-DPS**.

The ground-state geometries of bis[4-(1,4-dimethyl-carbazole)phenyl]sulfone (**DMCZ-DPS**) and bis[4-(9,9-dimethyl-9,10-dihydroacridine)phenyl]sulfone (**DMAC -DPS**) were optimized using density functional theory (DFT) at the B3LYP/6-31G* level, and compared with that of **DTC-DPS** (Fig. 4-2). By changing donor units from 3,6-di-tertbutylcarbazole (**DTC**) to 1,4-dimethyl-9H-carbazole (**DMCZ**), the dihedral angles between donor and acceptor planes were significantly increased due to the increase of the steric hindrance induced by the methyl groups. According to the calculation result, the dihedral angle between the donor and acceptor units in **DMCZ-DPS** and **DMAC-DPS** are 65° and 89°, respectively, which are much larger than that of 50° in **DTC-DPS**. As a result, HOMO and LUMO distributions are efficiently separated in both **DMCZ-DPS** and **DMAC-DPS**. The singlet-triplet splitting of the HOMO→LUMO (CT) transition was calculated to be 0.01 eV for both **DMCZ-DPS** and **DMAC-DPS**, which is much smaller than that of 0.34 eV for **DTC-DPS**, although it is insufficient to ensure that a ^{3}CT state is the T_1 only by a simulation based on TD-DFT/B3LYP/6-31G*.
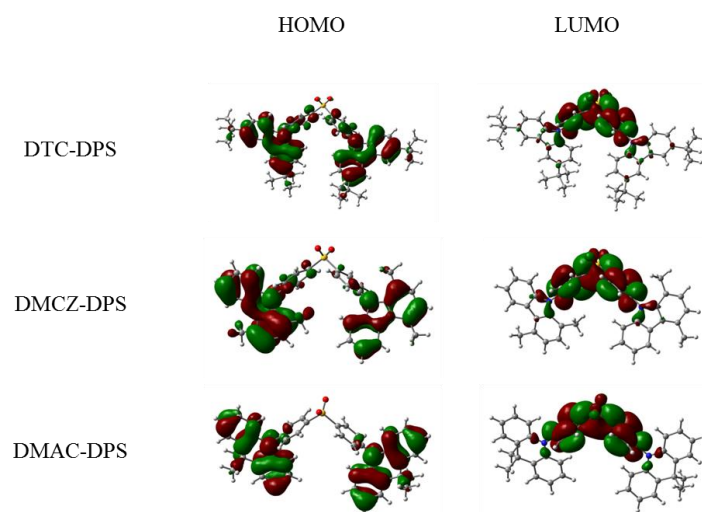

Figure 4-3. HOMO and LUMO distributions of **DTC-DPS**, **DMCZ-DPS** and **DMAC-DPS** calculated at the B3LYP/6-31G(d) level.

4.3 Photophysical characteristics

The low-lying energy levels and photophysical properties of **DTC-DPS**, **DMCZ-DPS** and **DMAC-DPS** were investigated in toluene. Fig. 4-4 demonstrates the absorption, fluorescence and phosphorescence spectra of the three compounds. The lowest-energy absorption peak appears at 350-370 nm can be assigned to the intramolecular charge transfer (ICT) transition because of the dipolar nature of these compounds. The low intensity of the CT band in the absorption spectrum of **DMAC-DPS** is consistent with the overlap-forbidden nature of the CT transition in **DMAC-DPS,** leading to a small transition dipole moment and low oscillator strength. At RT, all three compounds exhibit broad and structureless emission bands with a maximum at 402-460 nm, which can be ascribed to the ICT transition. At 77 K, the phosphorescence spectrum of **DMAC-DPS** is also broad and structureless, indicating a CT character of its T_1 state. In contrast, the phosphoresce spectra of **DTC-DPS** and **DMCZ-DPS** demonstrate a well resolved structure, indicating that the T_1 states of these two compounds are $^3\pi$-π states localized on the carbazole subunits. The shortest peak wavelength of the well resolved phosphoresce spectra was used to determine the $^3\pi$-π* level and the onset of the CT spectra were used to determine the ^{1}CT and ^{3}CT levels.[18, 24, 25] The singlet and triplet levels of **DTC-DPS**, **DMCZ-DPS** and **DMAC-DPS** are therefore estimated to be 3.32/2.97 eV (ΔE_{ST} = 0.35 eV), 3.32/2.97 eV (ΔE_{ST} = 0.35 eV) and 3.00 /2.97 eV (ΔE_{ST} = 0.03 eV), respectively.
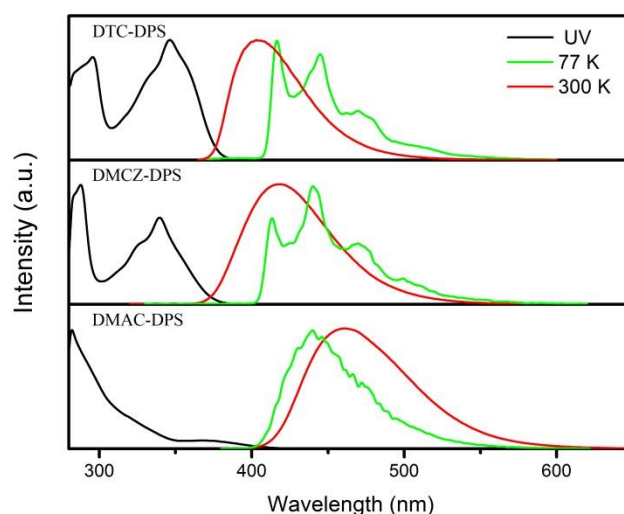
Figure 4-4. The absorption, fluorescence and phosphorescence spectra of **DTC-DPS, DMCZ-DPS** and **DMAC-DPS** in toluene.
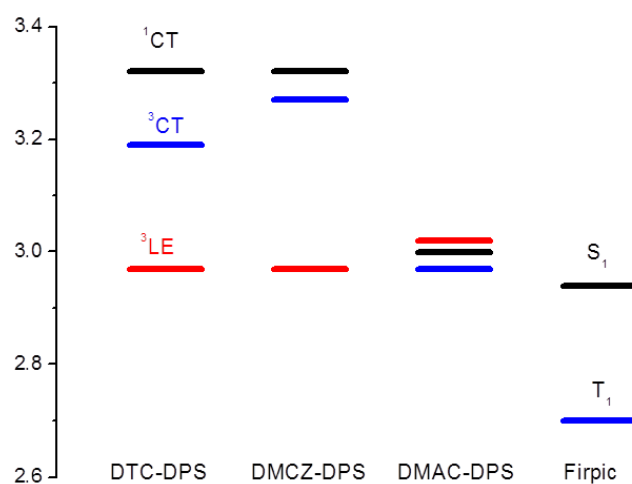

Figure 4-5. The excited state energies of ^{1}CT, ^{3}CT and ^{3}LE states of **DTC-DPS**, **DMCZ-DPS**, **DMAC-DPS** and **FIrpic**. The 0-0´ energy of ^{1}CT state are determined from the fluorescence spectrum in toluene at RT, while that of the ^{3}LE state is determined from the phosphorescence spectra in toluene at 77 K (Fig. 4-4). The energy differences between ^{1}CT and ^{3}CT states are derived from the computational prediction. The data of **FIrpic** is cited from previous work.[26]

Photophysical data of **DTC-DPS**, **DMCZ-DPS** and **DMAC-DPS** in oxygen-free toluene at RT are listed in Table 4-1. The transient PL decay of **DMAC-DPS** includes

a prompt fluorescence component with a lifetime of 20 ns and a delayed TADF component with a lifetime of 7.1 µs. Owing to the much smaller ΔE_{ST} of **DMAC-DPS**, this TADF lifetime is much shorter than that observed for **DTC-DPS** at the same condition (270 µs).[21, 24, 27, 28] However, we can hardly observe delayed component in the decay spectra of **DMCZ-DPS**. In addition, the total PL quantum yield (Φ) of 0.26 for **DMCZ-DPS** in oxygen-free toluene is also much lower than that of 0.80 for **DMAC-DPS**. Obviously, the low-lying ^{3}LE states prevent efficient repopulation of the emissive ^{1}CT state for **DMCZ-DPS**. Instead, the energy from ^{3}LE state dissipates by nonradiative processes. Similarly, the delayed component for **DTC-DPS** is very weak in solution because of its large ΔE_{ST}. The higher Φ_F of **DTC-DPS** relative to **DMCZ-DPS** would be due to its higher rate constants of fluorescence (k_F), which is proportional to Φ_F through equation (1).[29]

$$\Phi_F = k_F/(k_F+k_{IC}+k_{ISC}) \quad (1)$$

Here k_{IC} and k_{ISC} are the rate constants of internal conversion and intersystem crossing, respectively. Using the rate constant data in Table 4-1 and equation (5) derived in Chapter 3, ΔE_{ST} of **DTC-DPS** and **DMCZ-DPS** are calculated to be 0.35 eV and 0.08 eV, respectively, which is in good agreement with the corresponding values determined from the fluorescence and phosphorescence spectra (Fig. 4-4).

Table 4-1. Photophysical data in oxygen-free toluene at RT.

Parameter	DTC-DPS	DMCZ-DPS	DMAC-DPS
$\lambda_{max,em}$ (nm)	404	418	460
Φ_F	0.65	0.26	0.16
Φ_{TADF}	0.04	–	0.64
τ_F (ns)	5.3	7.9	20
τ_{TADF} (µs)	270	–	7.1
k_F (s^{-1})	1.2×10^8	3.3×10^7	8.0×10^6
k_{TADF} (s^{-1})	1.5×10^2	–	9.0×10^4
ΔE_{ST} (eV)	0.35	–	0.08

The photophysical properties of **DTC-DPS**, **DMCZ-DPS** and **DMAC-DPS** doped into **DPEPO** films at a concentration of 10 wt% was investigated by a streak camera coupled to a monochromator and using a nitrogen laser (λ=337 nm, pulse width of ~300 ps, repetition rate of 20 Hz) as the excitation source. The streak images are shown in Fig. 4-6 and the photophysical data are summarized on Table 4-2.

Table 4-2. Photophysical data of **DTC-DPS**, **DMCZ-DPS** and **DMAC-DPS** in 10 wt%-doped **DPEPO** films at RT.

Parameter	DTC-DPS	DMCZ-DPS	DMAC-DPS
$\lambda_{max,em}$ (nm)	410	430	470
Φ_F	0.64	0.39	0.30
Φ_{TADF}	0.16	0.13	0.60
τ_F (ns)	7.6	25	20
τ_{TADF} (μs)	1330	98	5.9
k_F (s^{-1})	8.4×10^7	1.6×10^7	1.5×10^7
k_{TADF} (s^{-1})	1.23×10^2	1.3×10^3	1.0×10^5
ΔE_{ST} (eV)	0.35	0.22	0.10

In comparison with the emission bands in toluene, the corresponding ones in **DPEPO** doped films are slightly red shifted. Because a rigid matrix suppresses collision-induced intramolecular radiationless transitions and bimolecular processes, the PLQYs of **DTC-DPS**, **DMCZ-DPS** and **DMAC-DPS** increase to 0.80, 0.52 and 0.90, respectively, in **DPEPO** films at RT. A clear delayed component is observed in the streak image of **DMAC-DPS** doped into **DPEPO** (Fig. 4-6). Moreover, the TADF component of **DTC-DPS** also increases in the doped film, because of the suppression of the non-radiative processes from T_1 to S_0. Since **DMAC-DPS** has a high quantum yield and large Φ_{TADF}/Φ_F ratio, $k_{ISC} > k_F >> k_{IC}$ is expected for it in the doped film. Thus, k_{ISC} of **DMAC-DPS** was estimated to be 3.5×10^7 s^{-1} by using an equation (2) simplified from equation (1):

$$\Phi_F = k_F/(k_F+k_{ISC}) \qquad (2)$$

Although this rate is markedly lower than those of transition metal complexes

$(10^{10}-10^{13} \text{ s}^{-1})$,[30, 31] it does not seem to prevent TADF emitters from realizing efficient k_{TADF}.
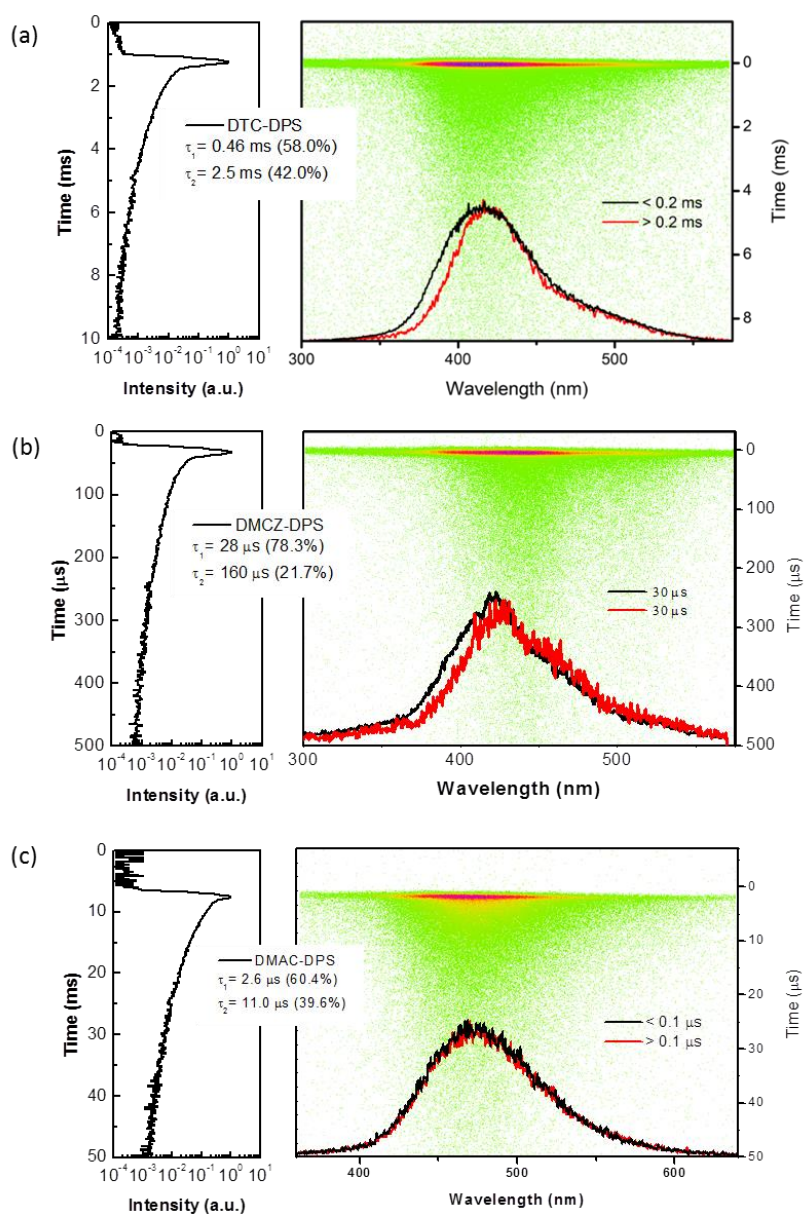

Figure 4-6. Streak images (transient PL decays) of **DTC-DPS** (a), **DMCZ-DPS** (b) and **DMAC-DPS** (c) doped into a **DPEPO** (10 wt%) film at room temperature.

The TADF decay of these compounds in doped films can be well fitted with double exponentials (Fig. 4-6), and their average lifetimes are listed in Table 4-2. On

the basis of the individual PLQYs of TADF (Φ_{TADF}) and the average TADF lifetime (τ_{TADF}), k_{TADF} of **DMAC-DPS** in a solid film was calculated to be as large as 1.5×10^7 s^{-1}, which is not only significantly higher than those of **DTC-DPS** and **DMCZ-DPS**, but also comparable with those of phosphorescent materials.[32] Therefore, the relaxation of the roll-off characteristics at high current density will be expected in a **DMAC-DPS** based OLED. As revealed by equation (5) in Chapter 3, a large k_F and a small ΔE_{ST} are two keys to realizing a large k_{TADF}. ΔE_{ST} of **DMAC-DPS** in doped film is thus calculated from k_{TADF} and k_F to be 0.10 eV, which is much smaller than that of 0.35 eV for **DTC-DPS** and 0.22 eV for **DMCZ-DPS**.

4.4 OLED performance

Since all these three compounds have high T_1 energies, a complicated device configuration of **ITO/α-NPD** (30 nm)/**TCTA** (20 nm)/**CzSi** (10 nm)/Emitter in **DPEPO** (10wt%, 15 nm)/**TPBI** (60 nm)/LiF (0.8 nm)/Al (100 nm) was utilized to realize efficient exciton confinement. Here, **α-NPD**, **TCTA**, **CzSi** and **TPBI** are N,N′-diphenyl-N,N′-bis(1-naphthyl)-1,10-biphenyl-4,4′-diamine,4,4′,4″-tris(N-carbazolyl)-triphenylamine, 9-(4-*tert*-butylphenyl)-3,6-bis(triphenylsilyl)-9*H*- carbazole and 1,3,5-tris(*N*-phenylbenzimidazol-2-yl)benzene, respectively (Fig. 4-7). As shown in Fig. 4-8, all EL spectra coincided well with their PL spectra. The EQEs of **DTC-DPS**, **DMCZ-DPS** and **DMAC-DPS** based OLEDs at 0.01 mA/cm^2 are 10%, 5.5% and 19.5%, respectively. The device containing **DMAC-DPS** having large k_{TADF} achieves small efficiency roll-off characteristics. Conversely, the devices with long-lived TADF emitters **DTC-DPS** and **DMCZ-DPS** exhibited considerable efficiency roll-off as expected. For comparison, a well-known blue phosphorescent emitter of bis[(4,6-difluorophenyl)pyridinato-N,C2](picolinato) iridium (**FIrpic**) was included in a device with the same structure. This device exhibits sky-blue emission with Commission Internationale de L'Eclairage (CIE) coordinates of (0.16, 0.34), in

contrast to that of (0.16, 0.20) for the **DMAC-DPS**-based device. Although the emission maxima of both devices are at 470 nm, the **DMAC-DPS**-based device offered better color purity because of a deep blue component at 400–450 nm in its EL spectrum (Fig. 4-8).
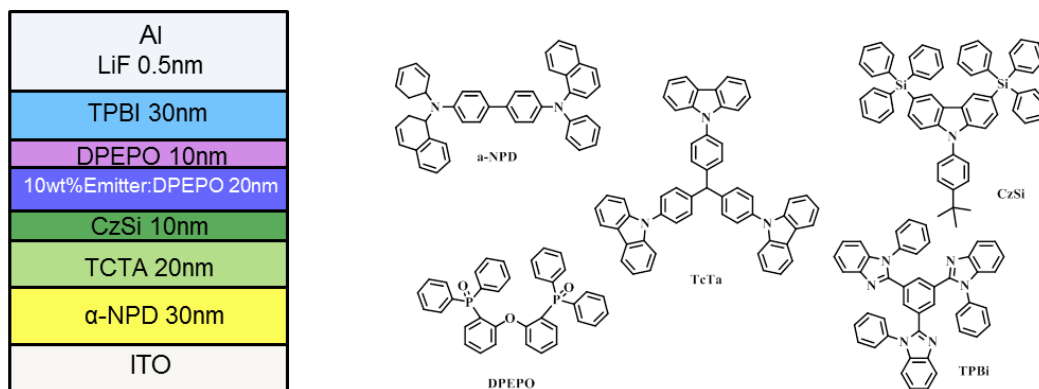

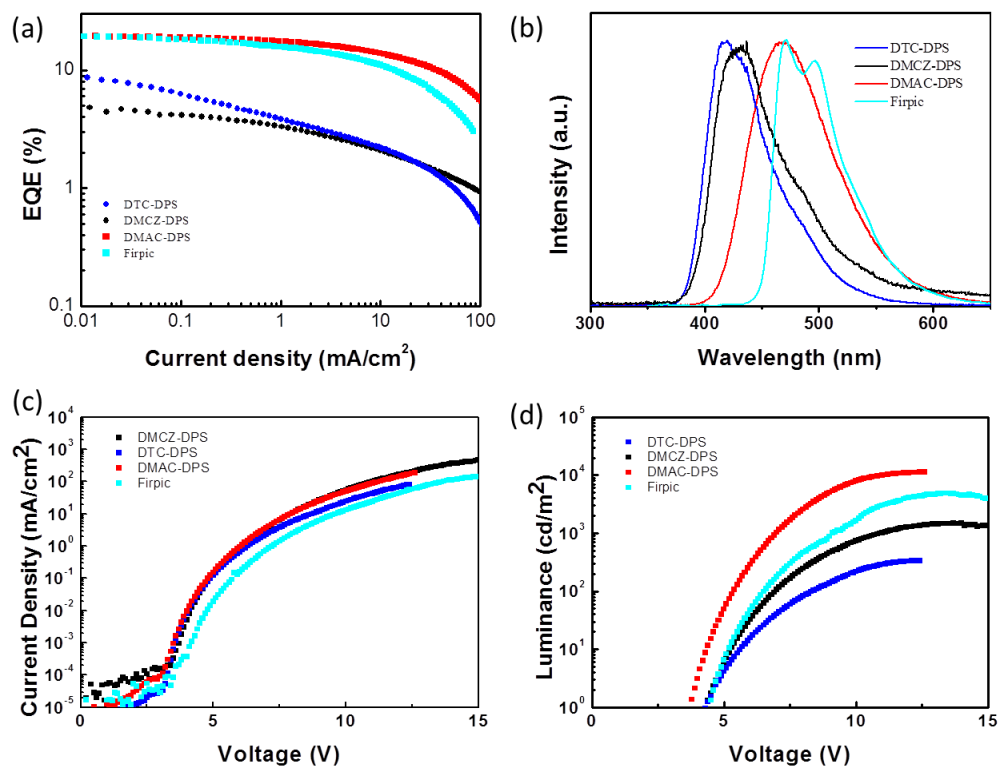**Figure 4-7**. Device structure of OLED and the chemical structures used in this study.

Figure 4-8. EQE–current density characteristics (a), electroluminescence spectra (b), current density–voltage characteristics (c) and luminance–voltage characteristics (d) of the above OLEDs.

The maximum EQE of the **FIrpic**-based OLED is close to that of the **DMAC-DPS**-based one, consistent with their similar PLQYs in a **DPEPO** host.[24] However, the **Firpic**-based OLED showed relatively low efficiency at high current density in our controlled experiment, along with higher turn-on and driving voltages than the **DMAC-DPS**-based OLED (Fig. 4-8). Because the excited-state lifetime of **Firpic** (~1 μs) is not longer than that of **DMAC-DPS** in doped films,[24] the more serious efficiency roll-off for the **FIrpic**-based OLED cannot be explained in the terms of the triplet-triplet annihilation, and is tentatively assigned to the decrease of charge balance at high current density,[33] taking into account the deeper HOMO level of **FIrpic** that can't reduce hole injection barrier to the EML (-6.1 eV for Firpic vs. -5.9 eV for **DMAC-DPS**, see Fig. 4-9).
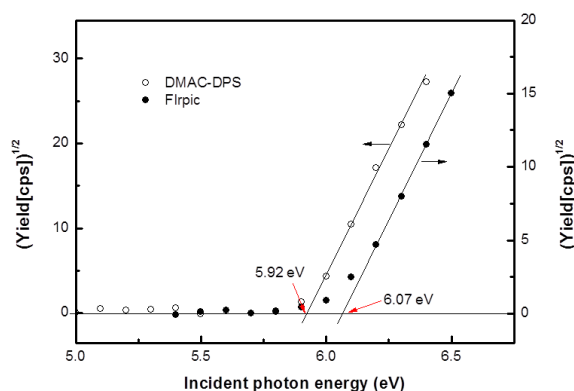

Figure 4-9. Photoelectron yield spectra of neat films of **DMAC-DPS** and **FIrpic**.

Although the above EL properties of **DMAC-DPS**-based OLED are comparable with those of the best deep blue PHOLEDs reported in recently,[5, 34, 35] its reliability is not superior to that of PHOLEDs at this stage. The half-life of both **FIrpic**- and **DMAC**-**DPS**-based devices is only 1 hour at an initial luminescence of 500 cd/m^2. However, blue phosphorescent emitters have been thoroughly studied over fifteen years. In contrast, TADF based OLEDs are still primitive stage and I can expect to realize long-living blue OLEDs based on the improved molecular structures of TADF

molecules and device architecture.[35]

4.5 Conclusion

In short, the PL and EL properties of three donor-acceptor type molecules with the same acceptor unit of diphenylsulphone (**DPS**) but different donor units of 3,6-di-tertbutylcarbazole (**DTC**), 1,4-Dimethyl-9H-carbazole (**DMCZ**) and 9,9-dimethyl-9,10-dihydroacridine (**DMAC**) were investigated in detailed. In comparison with **DTC-DPS**, the dihedral angles between the donor and acceptor units in **DMCZ-DPS** and **DMAC-DPS** are large, leading to small singlet-triplet CT state splitting. However, only **DMAC-DPS** can emit efficient and short-lifetime (a few microseconds) TADF, because the ^{3}CT state is its lowest triplet state. For both **DTC-DPS** and **DMCZ-DPS**, their T_1 states were found to be a $^3\pi$-π^* state localized at the carbazole units. We demonstrate that a pure organic aromatic emitter, **DMAC-DPS**, can achieve high EL performance that is comparable to today's best blue PHOLEDs, indicating that developing TADF materials can be a promising approach to the realization of low-cost and high-performance blue OLEDs.

References

1. Orselli, E.; Kottas, G. S.; Konradsson, A. E.; Coppo, P.; Fröhlich, R.; De Cola, L.; van Dijken, A.; Büchel, M.; Börner, H., Blue-Emitting Iridium Complexes with Substituted 1,2,4-Triazole Ligands: Synthesis, Photophysics, and Devices. *Inorganic Chemistry* **2007,** *46*, 11082-11093.

2. Liao, L. S.; Klubek, K. P., Power efficiency improvement in a tandem organic light-emitting diode. *Applied Physics Letters* **2008,** *92*, 223311.

3. Sajoto, T.; Djurovich, P. I.; Tamayo, A. B.; Oxgaard, J.; Goddard, W. A.; Thompson, M. E., Temperature Dependence of Blue Phosphorescent Cyclometalated Ir(III) Complexes. *Journal of the American Chemical Society* **2009,** *131*, 9813-9822.

4. Yook, K. S.; Jeon, S. O.; Joo, C. W.; Lee, J. Y., High efficiency deep blue phosphorescent organic light-emitting diodes. *Organic Electronics: physics, materials, applications* **2009,** *10*, 170-173.

5. Jeon, S. O.; Jang, S. E.; Son, H. S.; Lee, J. Y., External Quantum Efficiency Above 20% in Deep Blue Phosphorescent Organic Light-Emitting Diodes. *Advanced Materials* **2011,** *23*, 1436-1441.

6. Yook, K.; Lee, J. H., Organic materials for deep blue phosphorescent organic light-emitting diodes. *Advanced materials (Deerfield Beach, Fla.)* **2012,** *24*, 3169-3190.

7. Yang, C. H.; Mauro, M.; Polo, F.; Watanabe, S.; Muenster, I.; Fröhlich, R.; De Cola, L., Deep-Blue-Emitting Heteroleptic Iridium(III) Complexes Suited for Highly Efficient Phosphorescent OLEDs. *Chemistry of Materials* **2012,** *24*, 3684-3695.

8. Hudson, Z. M.; Sun, C.; Helander, M. G.; Chang, Y. L.; Lu, Z. H.; Wang, S., Highly Efficient Blue Phosphorescence from Triarylboron-Functionalized Platinum(II) Complexes of N-Heterocyclic Carbenes. *Journal of the American Chemical Society* **2012,** *134*, 13930-13933.

9. Fan, C.; Li, Y. H.; Yang, C. L.; Wu, H. B.; Qin, J. G.; Cao, Y., Phosphoryl/Sulfonyl-Substituted Iridium Complexes as Blue Phosphorescent Emitters for Single-Layer Blue and White Organic Light-Emitting Diodes by Solution Process. *Chemistry of Materials* **2012,** *24*, 4581-4587.

10. Sajoto, T.; Djurovich, P. I.; Tamayo, A.; Yousufuddin, M.; Bau, R.; Thompson, M. E.; Holmes, R. J.; Forrest, S. R., Blue and Near-UV Phosphorescence from Iridium Complexes with Cyclometalated Pyrazolyl or N-Heterocyclic Carbene Ligands. *Inorganic Chemistry* **2005,** *44*, 7992-8003.

11. Hu, J.-Y.; Pu, Y.-J.; Satoh, F.; Kawata, S.; Katagiri, H.; Sasabe, H.; Kido, J., Bisanthracene-Based Donor–Acceptor-type Light-Emitting Dopants: Highly Efficient Deep-Blue Emission in Organic Light-Emitting Devices. *Advanced Functional Materials* **2014,** *24*, 2064-2071.

12. Zhang, P.; Dou, W.; Ju, Z.; Yang, L.; Tang, X.; Liu, W.; Wu, Y., A 9, 9′-bianthracene-cored molecule enjoying twisted intramolecular charge transfer to enhance radiative-excitons generation for highly efficient deep-blue OLEDs. *Organic Electronics* **2013,** *14*, 915-925.

13. Li, W.; Liu, D.; Shen, F.; Ma, D.; Wang, Z.; Feng, T.; Xu, Y.; Yang, B.; Ma, Y., A twisting donor-acceptor molecule with an intercrossed excited state for highly efficient, deep-blue electroluminescence. *Advanced Functional Materials* **2012,** *22*, 2797-2803.

14. Kim, B.; Park, Y.; Lee, J.; Yokoyama, D.; Lee, J. H.; Kido, J.; Park, J., Synthesis and electroluminescence properties of highly efficient blue fluorescence emitters using dual core chromophores. *Journal of Materials Chemistry C* **2013,** *1*, 432-440.

15. Kondakov, D. Y.; Pawlik, T. D.; Hatwar, T. K.; Spindler, J. P., Triplet annihilation exceeding spin statistical limit in highly efficient fluorescent organic light-emitting diodes. *Journal of Applied Physics* **2009,** *106*, 124510.

16. Endo, A.; Ogasawara, M.; Takahashi, A.; Yokoyama, D.; Kato, Y.; Adachi, C., Thermally activated delayed fluorescence from Sn(4+)-porphyrin complexes and their application to organic light emitting diodes--a novel mechanism for electroluminescence. *Advanced Materials* **2009,** *21*, 4802-4806.

17. Tanaka, H.; Shizu, K.; Nakanotani, H.; Adachi, C., Twisted Intramolecular Charge Transfer State for Long-Wavelength Thermally Activated Delayed Fluorescence. *Chemistry of Materials* **2013,** *25*, 3766-3771.

18. Zhang, Q.; Li, J.; Shizu, K.; Huang, S.; Hirata, S.; Miyazaki, H.; Adachi, C., Design of efficient thermally activated delayed fluorescence materials for pure blue organic light emitting diodes. *Journal of the American Chemical Society* **2012,** *134*, 14706-14709.

19. Goushi, K.; Yoshida, K.; Sato, K.; Adachi, C., Organic light-emitting diodes employing efficient reverse intersystem crossing for triplet-to-singlet state conversion. *Nature Photonics* **2012,** *6*, 253-258.

20. Nakagawa, T.; Ku, S. Y.; Wong, K. T.; Adachi, C., Electroluminescence based on thermally activated delayed fluorescence generated by a spirobifluorene donor-acceptor structure. *Chemical Communications* **2012,** *48*, 9580-9582.

21. Tanaka, H.; Shizu, K.; Miyazaki, H.; Adachi, C., Efficient green thermally activated delayed fluorescence (TADF) from a phenoxazine-triphenyltriazine (PXZ-TRZ) derivative. *Chemical Communications* **2012,** *48*, 11392-11394.

22. Zhang, Y.; Lai, S. L.; Tong, Q. X.; Lo, M. F.; Ng, T. W.; Chan, M. Y.; Wen, Z. C.; He, J.; Jeff, K. S.; Tang, X. L.; Liu, W. M.; Ko, C. C.; Wang, P. F.; Lee, C. S., High Efficiency Nondoped Deep-Blue Organic Light Emitting Devices Based on Imidazole-π-triphenylamine Derivatives. *Chemistry of Materials* **2012,** *24*, 61-70.

23. Ford, W. E.; Rodgers, M. A. J., Reversible Triplet Triplet Energy-Transfer within a Covalently Linked Bichromophoric Molecule. *Journal of Physical Chemistry* **1992,** *96*, 2917-2920.

24. Zhang, Q. S.; Komino, T.; Huang, S. P.; Matsunami, S.; Goushi, K.; Adachi, C., Triplet Exciton Confinement in Green Organic Light-Emitting Diodes Containing Luminescent Charge-Transfer Cu(I) Complexes. *Advanced Functional Materials* **2012,** *22*, 2327-2336.

25. Huang, S.; Zhang, Q.; Shiota, Y.; Nakagawa, T.; Kuwabara, K.; Yoshizawa, K.; Adachi, C., Computational Prediction for Singlet- and Triplet-Transition Energies of Charge-Transfer Compounds. *Journal of Chemical Theory and Computation* **2013,** *9*, 3872-3877.

26. Wu, J.; Wu, S.-X.; Wu, Y.; Kan, Y.-H.; Geng, Y.; Su, Z.-M., Quantum chemical characterization and design of host materials based on phosphine oxide-substituted (triphenylamine) fluorene for (deep) blue phosphors in OLEDs. *Physical Chemistry Chemical Physics* **2013,** *15*, 2351-2359.

27. Lee, J.; Shizu, K.; Tanaka, H.; Nomura, H.; Yasuda, T.; Adachi, C., Oxadiazole- and triazole-based highly-efficient thermally activated delayed fluorescence emitters for organic light-emitting diodes. *Journal of Materials Chemistry C* **2013,** *1*, 4599-4604.

28. Wu, S.; Aonuma, M.; Zhang, Q.; Huang, S.; Nakagawa, T.; Kuwabara, K.; Adachi, C., High-efficiency deep-blue organic light-emitting diodes based on a thermally activated delayed fluorescence emitter. *Journal of Materials Chemistry C* **2014,** *2*, 421-424.

29. Klessinger, M.; Michl, J., *Excited states and photochemistry of organic molecules*. VCH: New York, 1995.

30. Yersin, H., *Highly efficient OLEDs with phosphorescent materials*. Wiley-VCH: Weinheim, 2008.

31. Hashimoto, M.; Igawa, S.; Yashima, M.; Kawata, I.; Hoshino, M.; Osawa, M., Highly Efficient Green Organic Light-Emitting Diodes Containing Luminescent Three-Coordinate Copper(I) Complexes. *Journal of the American Chemical Society* **2011,** *133*, 10348-10351.

32. Kawamura, Y.; Brooks, J.; Brown, J. J.; Sasabe, H.; Adachi, C., Intermolecular Interaction and a Concentration-Quenching Mechanism of Phosphorescent Ir(III) Complexes in a Solid Film. *Physical Review Letters* **2006,** *96*, 017404.

33. Giebink, N. C.; Forrest, S. R., Quantum efficiency roll-off at high brightness in fluorescent and phosphorescent organic light emitting diodes. *Physical Review B* **2008,** *77*, 235215.

34. Hang, X.-C.; Fleetham, T.; Turner, E.; Brooks, J.; Li, J., Highly Efficient Blue-Emitting Cyclometalated Platinum(II) Complexes by Judicious Molecular Design. *Angewandte Chemie International Edition* **2013,** *52*, 6753-6756.

35. Lee, S.; Kim, S.-O.; Shin, H.; Yun, H.-J.; Yang, K.; Kwon, S.-K.; Kim, J.-J.; Kim, Y.-H., Deep-Blue Phosphorescence from Perfluoro Carbonyl-Substituted Iridium Complexes. *Journal of the American Chemical Society* **2013,** *135*, 14321-14328.

Chapter 5

Summary and conclusions

In this thesis, I proposed a new scheme to obtain high efficiency blue OLEDs employing thermal activated delayed fluorescence (TADF). The PL and EL mechanism of TADF was introduced in Chapter 1. A small energy difference between the lowest singlet and triplet excited-states (ΔE_{ST}) was considered to be an important factor to reach TADF in pure organic aromatic compounds. CT compounds with sufficiently separated HOMO and LUMO were found to be promising candidates for the realization of TADF. However, a systemic study in this thesis reveals that the T_1 state of most CT compounds is a locally excited triplet state (^3LE). Efficient TADF can only be realized when the energy gap between ^1CT and ^3CT states is small enough and the energy of any ^3LE state is higher than that of the ^3CT state. On the basis of this concept, I achieved efficient blue TADF from a CT molecule with a large twist angle and short conjugation length of both donor (D) and acceptor (A) units.

In Chapter 2, bluish green to red TADF emission was demonstrated from four pretwisted intramolecular CT molecules that have the same donor of 5-phenyl-5,10-dihydrophenazine (**PPZ**) but different acceptor unities. These compounds have small singlet–triplet CT state splitting but different energy relationships between ^3CT and ^3LE states. The T_1 state of the red emitter **PPZ-TRZ** is a ^3CT state, while that of other three emitter is a $^3\pi$-π* state localized on a **PPZ** unit. However, for the yellow emitting **PPZ-DPO**, its ^3CT state was close to its ^3LE state. As a result, **PPZ-TRZ** and **PPZ-DPO** emitted short-lifetime TADF and their devices showed reduced efficiency roll-off at high current density. In contrast, the large ΔE_{ST} in green and bluish green emitting **PPZ** derivatives, **PPZ-3TRZ** and **PPZ-4TRZ**, leads to inefficient energy up-conversion from their T_1 to S_1 states and very long TADF lifetimes in the doped films. Their OLEDs also suffer serious efficiency roll-off.

In Chapter 3, blue and bluish green TADF emissions were demonstrated from four monomeric and dimeric carbazolylcyanobenzenes. By changing the substitution position of the cyano groups on the phenyl rings, the twisting angle between the donor

and acceptor moieties could be adjusted. Ortho-substitution was found to lead to a larger twisting angle and a more efficient separation of the HOMO and LUMO. For the two dimeric carbazolylcyanobenzenes whose ^{3}LE states are higher than their ^{3}CT state, 2,6-dicyano substituted derivative (**3-bis-2-CzIPN**) gave a smaller ΔE_{ST}, a fast TADF decay rate, and reduced EL efficiency roll-off at high current density, as compared with the analogous 3,5-dicyano substituted derivative (**3-bis-5-CzIPN**).

In Chapter 4, the PL and EL properties of three blue emitting TADF compounds were investigated in detail. These three bipolar molecules have the same acceptor unit of diphenylsulphone (**DPS**) but the different donor units of 3,6-di-tertbutylcarbazole (**BCZ**), 1,4-dimethyl-9H-carbazole (**DMCZ**) and 9,9-dimethyl-9,10-dihydroacridine (**DMAC**). In comparison with **BCZ-DPS**, the dihedral angles between the donor and acceptor units in **DMCZ-DPS** and **DMAC–DPS** are larger, leading to small singlet–triplet CT state splitting. However, only **DMAC–DPS** can emit efficient and short-lifetime (a few microseconds) TADF because the ^{3}CT state is its lowest triplet state. The device based on **DMAC–DPS** offers an EQE of 19.5% and reduced efficiency roll-off characteristics at high luminance, which are comparable to that of today's best blue phosphorescent OLEDs, confirming that TADF materials can realize high- performance blue OLEDs.

Although efficient blue TADF based OLEDs have finally been demonstrated, it should be pointed out that the color purity and lifetime of the devices need to be further improved. The relatively broad PL band and large Stokes-shift for **DMAC–DPS** are related with the relatively large configuration distortion in the excited state. We believe increasing the rigidity of the acceptor moiety and preventing the D-A rotation by the introduction of steric hindrance groups can enable the emitter higher color purity without an increase of the band gap. To improve the reliability of blue TADF based OLEDs, we should develop new emitters with better electrochemical and excited sate stabilities. On the other hand, analogous to blue phosphorescent OLEDs, the development of high triplet energy charge transfer materials with moderate energy

gap and high charge mobility could be an approach to achieve stable blue TADF OLEDs.

Future OLEDs should be not only more efficient and more long-lived, but also more simple and cheaper. Encouraged by the fast growing efficiency of perovskite based solar cells[1, 2], a wide-ranging rethink of organic-inorganic hybrid OLEDs is also necessary. I think replacing some charge injection and transport materials as well as host materials by inorganic semiconductor compounds may be beneficial to the stability of TADF based OLEDs.

References

1.   Burschka, J.; Pellet, N.; Moon, S. J.; Humphry-Baker, R.; Gao, P.; Nazeeruddin, M. K.; Gratzel, M., Sequential deposition as a route to high-performance perovskite-sensitized solar cells. *Nature* **2013,** *499*, 316-319.

2.   Liu, M. Z.; Johnston, M. B.; Snaith, H. J., Efficient planar heterojunction perovskite solar cells by vapour deposition. *Nature* **2013,** *501*, 395-398.

Publication list

1. **<u>Li, B</u>**.; Nomura, H.; Miyazaki, H.; Zhang, Q.; Yoshida, K.; Suzuma, Y.; Orita, A.; Otera, J.; Adachi, C., Dicarbazolyldicyanobenzenes as Thermally Activated Delayed Fluorescence Emitters: Effect of Substitution Position on Photoluminescent and Electroluminescent Properties. *Chemistry Letters* **2014,** *43*, 319-321.

2. Zhang, Q.*; **<u>Li, B</u>**.*; Huang, S.; Nomura, H.; Tanaka, H.; Adachi, C., Efficient blue organic light-emitting diodes employing thermally activated delayed fluorescence. *Nature Photonics* **2014,** *8*, 326-332. (*: these authors contributes equally)

International conferences

1. **<u>Li, B</u>**.; Nomura, H.; Miyazaki, H.; Zhang, Q.; Yoshida, K.; Suzuma, Y.; Orita, A.; Otera, J.; Adachi, C., Dicarbazolyldicyanobenzenes as Thermally Activated Delayed Fluorescence Emitters: Effect of Substitution Position on Photoluminescent and Electroluminescent Properties. *Asian Conference on Organic Electronics* **2013, 13th-15th Nov.,** Pohang.

2. **<u>Li, B</u>**.; Nomura, H.; Miyazaki, H.; Zhang, Q.; Yoshida, K.; Suzuma, Y.; Orita, A.; Otera, J.; Adachi, C., Dicarbazolyldicyanobenzenes as Thermally Activated Delayed Fluorescence Emitters: Effect of Substitution Position on Photoluminescent and Electroluminescent Properties. *TADF workshop* **2014, 14th Mar.**, Fukuoka

Acknowledgements